

Spectroscopy, Dynamics and Hydration of S-Nitrosylated Myoglobin

Haydar Taylan Turan¹ and Markus Meuwly^{1*}

¹*Department of Chemistry, University of Basel, Klingelbergstrasse 80, Basel, Switzerland*

E-mail: m.meuwly@unibas.ch

Abstract

S-nitrosylation, the covalent addition of NO to the thiol side chain of cysteine, is an important post-translational modification that can alter the function of various proteins. The structural dynamics and vibrational spectroscopy of S-nitrosylation in the condensed phase is investigated for the methyl-capped cysteine model system and for myoglobin. Using conventional point charge and physically more realistic multipolar force fields for the -SNO group it is found that the SN- and NO-stretch and the SNO-bend vibrations can be located and distinguished from the other protein modes for simulations of MbSNO at 50 K. The finding of stable cis- and trans-MbSNO is consistent with experiments on other proteins as is the observation of buried -SNO. For MbSNO the observed relocation of the EF loop in the simulations by ~ 3 Å is consistent with the available X-ray structure and the conformations adopted by the -SNO label are in good overall agreement with the X-ray structure. Despite the larger size of the -SNO group, MbSNO is found to recruit more water molecules within 10 Å of the modification site than WT Mb due to the stronger electrostatics. Similarly, when comparing the hydration between the A- and H-helices they differ by up to 30 % between WT and MbSNO. This suggests that local hydration can also be significantly modulated through nitrosylation.

1 Introduction

Nitric oxide (NO) is a cell-signaling molecule relevant to function in the cardiovascular, nervous and immune systems.¹ Due to its high biological activity and diffusibility, NO plays an important role in many biological functions ranging from immune response, regulation of blood pressure to its function as a neurotransmitter.^{2,3} Furthermore, its reversible binding to ferrous or ferric heme iron is well characterized.⁴ One of the well known effects of NO on muscle tissue is the activation of guanylate cyclase by the binding of NO to the Heme group, which leads to relaxation of the smooth muscle.⁵ In addition, NO can also play an important role in post-translational modifications (PTM) of its target protein.⁶

S-Nitrosylation, i.e. the covalent addition of NO to the thiol side chain of cysteine, is an important PTM that mediates signal transduction. More than 3000 proteins, which are responsible for a wide range of cellular functions, have been identified as candidates for S-nitrosylation under physiological conditions.⁷ S-nitrosylation is reversible, precisely targeted and regulated by temporal and spatial arrangements. Specificity of S-Nitrosylation can be governed by acid-base motifs i.e. electrostatic interactions that affect the pK_a of thiol, and the physiological concentration of NO.⁸ Further, the relative hydrophobicity of the surrounding region of the thiol may provide 'hydrophobic motifs' that affect solvent and co-factor accessibility.⁹ Moreover, S-nitrosylation is known to alter the function of a protein via allosteric regulation¹⁰⁻¹³ and can inhibit or promote the formation of sulfide linkage within or between proteins.⁹

A number of studies have been proposed to characterize the underlying molecular mechanism of S-Nitrosylation. One of them is based on S-N decomposition that leads to thiyl radical

formation, and thiol deprotonation as a first step.¹⁴ Alternatively, a mechanism by which NO reacts directly with reduced thiol to generate a radical intermediate was proposed,¹⁵ or NO₂ reacts with thiol to produce thiyl radical intermediate, subsequently attacked by NO radical to form nitrosothiol.¹⁶ Finally, co-localization of nitric oxide synthase (NOS) enzymes with target protein found to be a determinant of S-nitrosylation under physiological conditions.¹⁷

Beside the actual mechanism for SNO formation, the detection of the final product is equally important. A wide range of indirect detecting techniques have been proposed, considered, and applied. They include the biotin-switch technique,¹⁸ His-tag switch¹⁹ or fluorogenic probes²⁰ which can be utilized to infer S-nitrosylation. Indirect methods usually break the S-N bond and capture the signals of the sulfur or nitrogen parts, instead of addressing the SNO adducts directly. However, such techniques have limitations and drawbacks in terms of their selectivity and reproducibility.²¹ Indirect methods need sequential manipulation before final analysis and can be hampered by decreasing chemoselectivity in each step.²² Also, interference of other species such as NO₂⁻ can yield artifacts in quantitative measurements.²³

Direct detection techniques such as gold nanoparticles (AuNP), phenylmercury, organophosphine or benzenesulfinate probes target the intact SNO moieties.²² One limitation is incomplete free thiol blockage which can lead to false positive results with AuNP.²⁴ Also, depending on the compound used as a probe, the general applicability can be limited due to toxicity, as is the case with phenylmercury.²² Further, it was reported that indirect sunlight can lead to reduction of biotin-HPDP to biotin-SH, and cause false-positives.²⁵

An alternative direct technique to demonstrate that S-nitrosylation has occurred is infrared (IR) spectroscopy. IR spectroscopy is a widely used technique for the structural characterization of proteins.^{26,27} Conformationally sensitive vibrations within the peptide backbone of the protein are the amide I (1600 to 1700 cm⁻¹), amide II (1510 to 1580 cm⁻¹), and

amide III (1200 to 1350 cm^{-1}) bands which report on the peptide backbone vibrations. As such, the method provides a structural fingerprint by which target proteins can be identified. Similarly, the SNO probe has the SN stretch, SNO bending and NO stretch modes which provide potentially useful signatures in the infrared to establish that S-nitrosylation has occurred. The main advantage of SNO is the chemical uniqueness of the probe. Only cysteine and methionine residues contain a sulfur atom and SN single and NO double bonds are absent in unmodified amino acids. On the other hand the frequency of the NO stretch mode at $\sim 1525\text{ cm}^{-1}$ overlaps with the amide-II band which makes it potentially challenging for direct detection.²⁸ There are also experimental difficulties to measure the IR spectrum of proteins in water. Due to the overlap between the HOH bending vibration of water and the conformationally sensitive amide II region at $\sim 1600\text{ cm}^{-1}$, the signals can be considerably improved by recording difference spectra for the ^{14}NO and ^{15}NO isotopes,²⁹ by subtracting the water background,^{30,31} or by subtracting the spectrum of the WT system.

Several studies examined the spectral³²⁻³⁷ and structural³⁸⁻⁴⁰ properties of S-Nitrosothiols in various media. The IR spectra of methyl thionitrites were studied in argon matrices at 12 K ³² and for ethyl thionitrites³³ in the gas phase for both, the cis- and trans-conformers of the two molecules. The NO stretch frequency was at 1527 cm^{-1} and 1537 cm^{-1} for the cis-, and at 1548 cm^{-1} and 1559 cm^{-1} for the trans- conformer for methyl-SNO in the argon matrix and for ethyl-SNO in the gas phase, respectively. Hence, for both systems the frequency of the trans- conformer is blue shifted with respect to the cis-orientation by 21 cm^{-1} and 22 cm^{-1} , respectively, whereas depending on the chemical environment the absolute frequencies vary by some 10 cm^{-1} . For S-nitrosogluthathione (GSNO) in solution only the cis-conformer was reported with a stretch frequency at 1497 cm^{-1} .⁴¹

Computational methods provide a viable alternative to investigate the relationship between structure, spectroscopy, and dynamics.⁴² Earlier investigations of the thiol group included

electronic structure studies of small model systems, such as CH_3SNO ^{38,39} or empirical force fields based on harmonic potentials using point charge (PC) models.^{43,44} In the present study, the spectral and structural properties of wild type (WT) blackfin tuna myoglobin (Mb) and its S-Nitrosylated analogue are studied by means of molecular dynamics simulations using Morse potentials and point charge and multipolar (MTP) force fields for the electrostatics. Two conformations of S-Nitrosylated myoglobin, *cis*-MbSNO and *trans*-MbSNO, with respect to the C_βSNO angle are considered. The aim is to characterize the absorption features in the infrared and the structural effects induced by S-Nitrosylation of Cys10. Changes in the local structure are potentially important for modifications in the function of a protein. Hence, the global and local dynamics of the protein and its helices and loops, and changes in the solvent shells around the protein are investigated.

The present work is structured as follows. First, the force field parametrization and the atomistic simulations are described. This is followed by the discussion of calculated IR and power spectra of the CysNO model system. Then, the IR spectra of WT, *cis*-MbSNO and *trans*-MbSNO are presented and discussed. Finally, structural effects induced by S-Nitrosylation are discussed and conclusions are drawn.

2 Computational Methods

2.1 Molecular Dynamics

All molecular Dynamics (MD) simulations were performed using the CHARMM⁴⁵ software with the CHARMM36⁴⁶ force field. The equations of motion were propagated with a leapfrog integrator,⁴⁷ using a time step of $\Delta t = 1$ fs and all bonds involving hydrogen atoms were constrained using SHAKE.⁴⁸ Non-bonded interactions were treated with a switch function⁴⁹ between 12 and 16 Å and electrostatic interactions were computed with the particle mesh

Ewald method.⁵⁰

Cys-NO: For simulating nitrosylated cysteine (Cys-NO), the molecule was placed in the center of a cubic box (dimensions $25 \times 25 \times 25 \text{ \AA}^3$) of TIP3P⁵¹ water and maintained there with a weak center-of-mass constraint with a force constant of 1 kcal/mol. Two sets of simulations were carried out: one using PC electrostatics and the other one with MTP interactions, see below. First, the systems were heated to 300 K and equilibrated at this temperature in the *NVT* ensemble for 500 ps. Production simulations of 10 ns were then performed in the *NVE* ensemble.

WT and Nitrosylated Mb: For the simulations involving wild type and S-nitrosylated Mb, eight different simulations were set up: wild-type myoglobin (PDB: 2NRL)⁵² at 50 K and 300 K, cis- and trans-S-Nitrosylated myoglobin (S-Nitrosylation at Cys10) with a PC model for the -SNO moiety at 50 K and 300 K, and cis- and trans-S-Nitrosylated myoglobin with a multipolar charge model at 50 K and 300K. Because density for the terminal residue Gly147 was missing in the 2NRL structure only residues Ala2 to Ser146 were used to set up the WT and S-nitrosylated protein at position Cys10. With this setup, simulations for cis-MbSNO and trans-MbSNO starting from the same initial structure except the dihedral angle $\phi(\text{C}_\beta\text{SNO})$ (0° for cis-MbSNO and 180° for trans-MbSNO) were started.

All systems were solvated in a $80 \times 80 \times 80 \text{ \AA}^3$ cubic box of TIP3P⁵¹ water molecules with buffer regions of 15 \AA to the edges of the box. The protein was weakly constrained to the middle of the simulation box, minimized, heated to the desired temperature and equilibrated for 500 ps in the *NVT* ensemble. Production runs of 10 ns were then performed in the *NVE* ensemble.

2.2 Parametrisation of the Force Field

The CHARMM36 force field was employed to describe the methyl-terminated Cys residue. The additional parameters required for Cys-NO were determined from electronic structure calculations. For this, the structure of $\text{H}_3\text{C}-\text{C}_3\text{H}_6\text{NO}_2\text{S}-\text{NO}$ was optimized at the MP2/aug-cc-pVDZ^{53,54} level of theory. All electronic structure calculations were carried out with Gaussian09.⁵⁵ The nature of the stationary point was verified by calculating vibrational frequencies. Then the SN bond was scanned along the bond separation r on a grid between 1.3 and 6 Å whereas the NO bond was scanned between 0.9 and 5.1 Å, both in increments of 0.1 Å. The coordinates of all atoms except for the NO moiety along the SN bond scan, and O for the NO bond scan were frozen.

Next, the reference MP2 energies were fit to Morse oscillator functions $V(r) = D_e[1 - \exp(-\beta(r - r_e))]^2$ where D_e is the well-depth, r_e is the equilibrium bond distance, and β is the parameter that controls the steepness of the potential. Subsequently, the steepness parameters β are adjusted such as to reproduce experimental frequencies of the SN and NO stretch vibrations at 520 and 1526 cm^{-1} , respectively.²⁸ The β values were 2.171 Å⁻¹ and 1.437 Å⁻¹ for the SN and NO stretch before fitted to the experimental vibration. For these parametrizations the energetically more stable cis-conformer was considered. The final Morse parameters after fitting β to the experimentally observed stretch frequencies are $D_e = 202.7$ kcal/mol, $\beta = 1.887$ Å⁻¹, $r_e = 1.207$ Å for the NO bond and $D_e = 71.1$ kcal/mol, $\beta = 1.987$ Å⁻¹, $r_e = 1.843$ Å for the SN bond.

For the SNO bending, the angle was scanned between 0° and 180°. For the bending potential, the reference energies were fitted to $V(\theta) = k_\theta(\theta - \theta_e)^2$ where k_θ is the force-constant and $\theta_e = 0$ is the equilibrium angle. Fitting the force constant to reproduce the experimentally determined frequency²⁸ of the SNO bending motion in GSNO at 886 cm^{-1} yields a value of $k_\theta = 132.5$ kcal/mol/rad² and $\theta_e = 115.6^\circ$.

For the electrostatic interactions two different models were developed. One of them is a standard point charge (PC) model and the second one uses multipoles (MTPs) on the S, N, and O atoms.^{56,57} For this, the charges of all atoms except for the S, N, and O atom (i.e. the -SNO label) were those of the CHARMM36 force field⁴⁶ which were kept constant. This was done in order to maintain the parametrization of the cysteine residue consistent with the remaining protein force field. On the other hand, the quality of the ESP fit will be affected by this strategy, see below. Two models were considered. The first is a PC model, fitted to the electrostatic potential (ESP) of the optimized structure of Cys-NO at the MP2/aug-cc-pVDZ level of theory, see Table 1. Next, these fitted PCs were frozen at the optimized values and the atomic dipole and quadrupole moments were fitted to improve the model.⁵⁸ All parameters are reported in Table 1.

The ESP maps for cis- and trans-CysNO with PCs and MTPs and the differences between the reference ESP (at the MP2 level) and those from the PC and MTP models are reported in Figures ?? and ?. The RMSE between reference ESP and the PC model is 8.36 kcal/mol and 7.44 kcal/mol for cis-CysNO and trans-CysNO, respectively. This rather larger difference originates from the fact that the CHARMM36 charges were retained and not allowed to adjust to the reference ESP in the fit. When including the MTPs on the -SNO label the RMSE decreased to 4.21 kcal/mol for cis-CysNO and 2.32 kcal/mol for trans-CysNO which is a significant improvement over a conventional PC model.

2.3 Infrared Spectrum

The infrared spectrum was obtained from the Fourier transform of the dipole moment autocorrelation function. For this, the molecular dipole moment was calculated from the MD trajectories and the partial charges. The autocorrelation function where i is the index num-

Table 1: The PC, dipole and quadrupole parameters generated at MP2/aug-cc-pVDZ level which been used in the MTP simulations

Parameter	PC [e]	Dipole [ea_0]			Quadrupole [ea_0^2]				
	Q_{00}	Q_{10}	Q_{1C}	Q_{1S}	Q_{20}	Q_{21C}	Q_{21S}	Q_{22C}	Q_{22S}
S	0.330	-0.373	0.079	0.000	0.032	0.006	0.000	-0.019	0.000
N	-0.203	0.000	0.359	0.128	0.370	0.000	0.000	-0.265	0.006
O	-0.127	0.104	-0.135	0.000	-0.040	0.040	0.000	-0.034	0.000

ber of a snapshot

$$C(t) = \sum_{i=1}^N \langle \vec{\mu}_i(0) \cdot \vec{\mu}_i(t) \rangle \quad (1)$$

was accumulated over 2^{15} time origins to cover 1/3 to 1/2 of the trajectory. From this, the absorption spectrum is determined according to

$$A(\omega) = \omega(1 - e^{-h\omega/(k_B T)}) \int C(t) e^{-i\omega t} dt \quad (2)$$

where T is the temperature in Kelvin, k_B is the Boltzmann constant and the integral is determined using a fast Fourier transform (FFT). IR spectra of WT, cis-MbSNO and trans-MbSNO have been generated for blocks of 100 ps simulation by correlating over 2^{19} time origins. A total of 100 spectra were generated for each system (total simulation time of 10 ns) and averaged.

Additionally power spectra of the NO and SN bonds and the SNO angle have been calculated from the FFT of the bond length and angle time series autocorrelation functions. This provides assignments of the vibrational spectra and allows to detect couplings between modes.⁵⁹ These power spectra were not averaged and correlated over 2^{15} time origins for the entire simulation time of 10 ns.

3 Results

First, the structural dynamics and IR spectroscopy of nitrosylated cysteine in solution was investigated. This provides a basis for characterization and interpretation the dynamics and spectroscopy of cysteine incorporated in a protein, such as myoglobin. Next, the spectroscopy and conformational dynamics of cis- and trans-MbSNO are discussed.

3.1 Dynamics and Spectroscopy of CysNO

Figure 1 shows the structure of cis-CysNO in aqueous solvent. Quantum chemical calculations at the MP2/aug-cc-pVDZ level show two minima with ϕ_{CSNO} dihedral angles of 0 and 180°. The energy profile $V(\phi)$ is reported in Figure ?? and shows a stability difference between the global minimum (cis-Cys-NO) and the trans-conformer ($\phi = 180^\circ$) of 2.5 kcal/mol with the two states separated by a barrier of ~ 15 kcal/mol at the MP2 level of theory. Hence, interconversion between the two states is expected to be slow and will be on the millisecond time scale according to transition state theory.

The IR and power spectra for Cys and CysNO are shown in Figure 2 and compared with the experimental line positions of the vibrations from Raman spectroscopy of S-nitrosoglutathione (GSNO) in the solid state²⁸ which was the reference for the parametrization. The NO stretch peak is clearly visible in Figure 2A at 1540 cm^{-1} for cis-CysNO and 1538 cm^{-1} for trans-CysNO (red and blue traces, respectively) as the power spectrum in Figure 2B confirms. Contrary to that, the SN and SNO peaks are more difficult to locate in the power spectrum. Considering the power spectra in Figures 2C and D, the SN stretch and SNO bending modes are at 514 cm^{-1} and 871 cm^{-1} for cis-CysNO and 495 cm^{-1} and 881 cm^{-1} for trans-CysNO, respectively, which are close to the experimental values. The power spectra (Figures 2B to D) show that SN and SNO modes are strongly coupled whereas the coupling to the NO

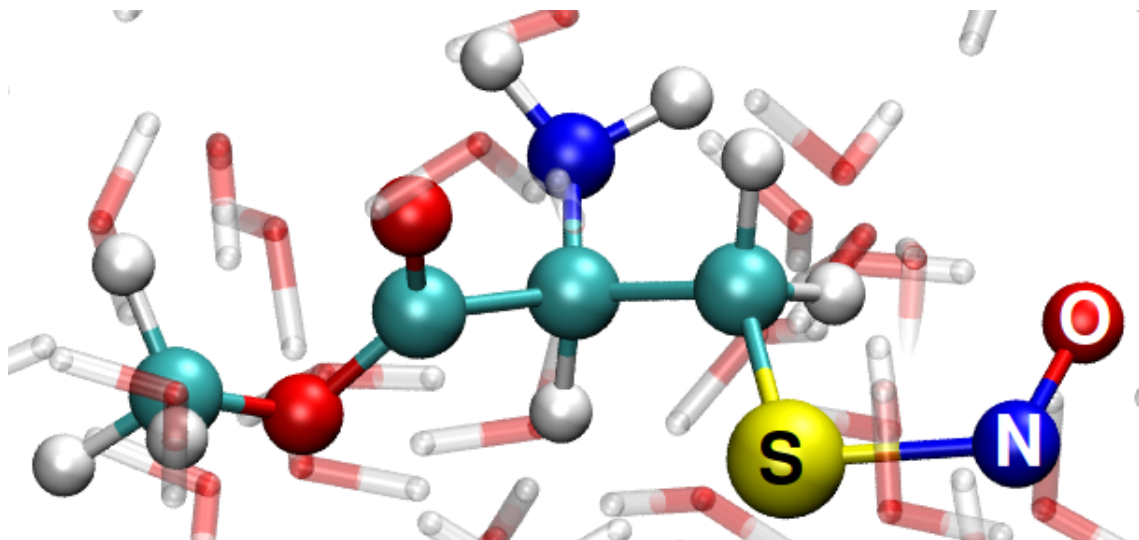


Figure 1: The structure of cis-CysNO in aqueous solvent. The CysNO ligand is shown as CPK and the TIP3P water molecules are drawn in licorice. The color code for the atoms is H (white), C (cyan), O (red), N (blue), S (yellow).

stretch is less pronounced.

Although the same force field was used for cis- and trans-CysNO, their spectroscopy for the SN and SNO modes differs. In the power spectra, the bands of trans-CysNO are red shifted by 29 cm^{-1} for SN and blue shifted by 14 cm^{-1} for SNO with respect to cis-CysNO, which should be sufficient to detect both isomers if they are present in solution. For the NO-stretch the splitting between cis- and trans-CysNO is 3 cm^{-1} in the gas phase which compares with 21 cm^{-1} for methyl thionitrite (CH_3SNO) in an Argon matrix³² whereas in solution, the present simulations only find an insignificant splitting. Consistent with experiment, the simulations also find that the trans-conformer absorbs at higher frequency. The different magnitude of the shift in the gas phase may be due to both, the different environment (argon in the experiments) and the somewhat different chemical environment of CH_3 versus Cysteine. Further, the SN stretch is at 376 cm^{-1} for cis- CH_3SNO and 371 cm^{-1} for trans- CH_3SNO which amounts to a red shift by 5 cm^{-1} .³² This shift was more pronounced in the present simulations with 29 cm^{-1} .

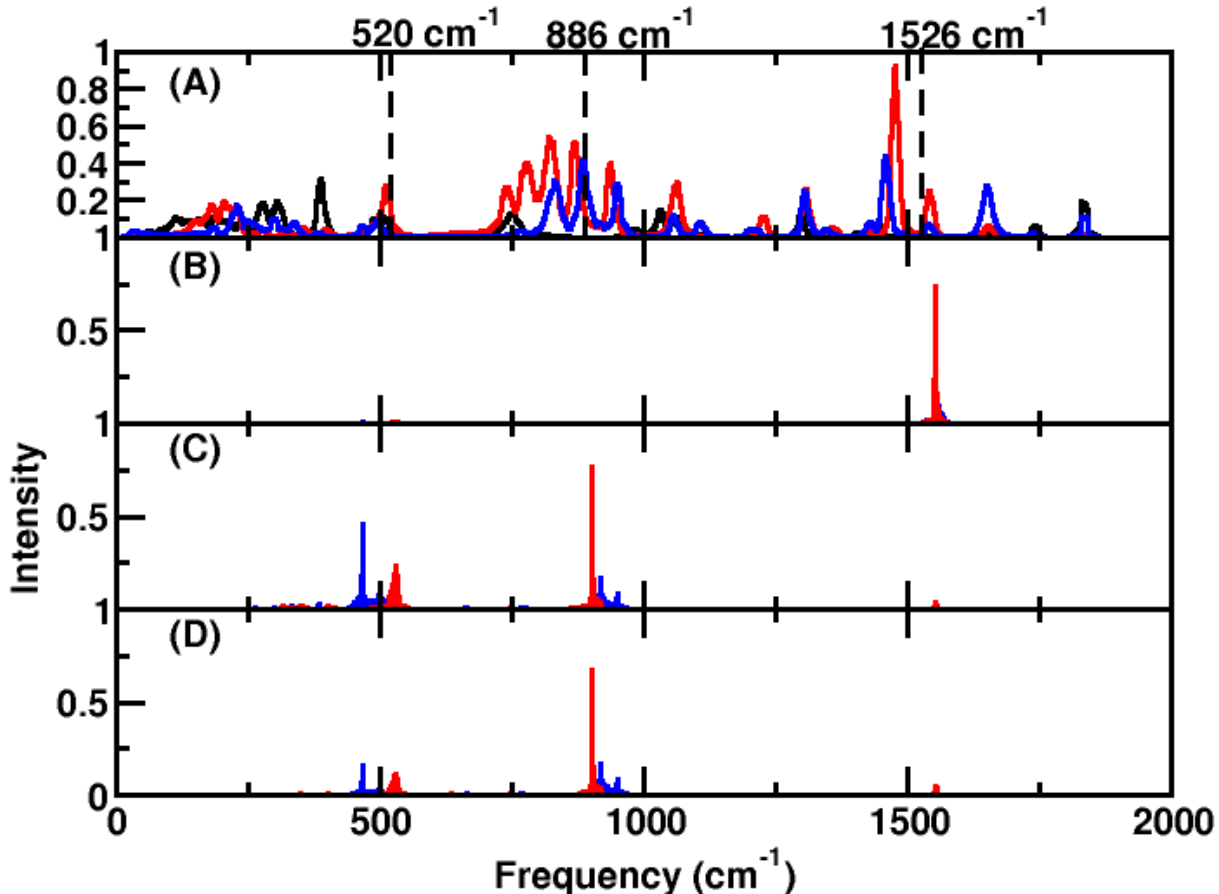


Figure 2: Infrared and power spectra for Cys (black) and Cys-NO (blue and red) in water. Panel A: calculated IR spectrum of Cys (Black), cis-Cys-NO (red) and trans-Cys-NO (blue) from the MD simulations at 50 K with the MTP model. Panels B to D: the NO, SNO and SN power spectra, respectively. The dashed lines at 520 cm⁻¹, 886 cm⁻¹ and 1526 cm⁻¹ are the experimental values for the SN, SNO and NO modes in GSNO in the solid state, respectively.²⁸ The dashed lines indicate the positions of the experimental values.

3.2 The Structural Dynamics and Spectroscopy of Mb-SNO

Next, the dynamics and spectroscopy of wild-type (WT) blackfin tuna myoglobin (PDB: 2NRL)⁵² and its S-nitrosylated variant⁵² at Cys10 (PDB: 2NRM) was considered, see Figure 3. For the S-nitrosylated cysteine in blackfin tuna myoglobin two different cis-conformers were reported.⁵² The major and minor cis- conformers had $\phi(\text{NC}_\alpha\text{C}_\beta\text{S})$ dihedral angles of -62° , 55° and $\phi(\text{C}_\alpha\text{C}_\beta\text{SN})$ of 172° , -72° in the X-Ray structures, respectively. In the simulations at 300 K with both, PC and MTP models, the structure with $\phi(\text{NC}_\alpha\text{C}_\beta\text{S}) \sim -62^\circ$ was present throughout the 10 ns simulation (see Figure ??B). With respect to the dihedral

$\phi(C_\alpha C_\beta SN)$, the simulation using MTPs sampled only the state with $\sim 160^\circ$ which is close to the major cis- conformer value whereas the simulation with PCs sampled both states with $\sim -85^\circ$ which is close to the minor cis- conformer value and $\sim 160^\circ$, see Figure ??A. The first, shorter lived state with $\phi(NC_\alpha C_\beta S) \sim -85^\circ$ using PCs was sampled for the first 2 ns after which $\phi(NC_\alpha C_\beta S)$ switched to $\sim 160^\circ$ and remained there for the rest of the simulation (see Figure ??B). These results indicate that the simulations are able to account for the major cis- conformer with both charge models at 300 K. Given the different spectroscopic features for cis- and trans-CysNO, for MbSNO also both conformers were considered in the MD simulations. The dynamics and spectroscopy of the WT and S-nitrosylated variants were studied at 50 K and 300 K using PC and MTP charge models.

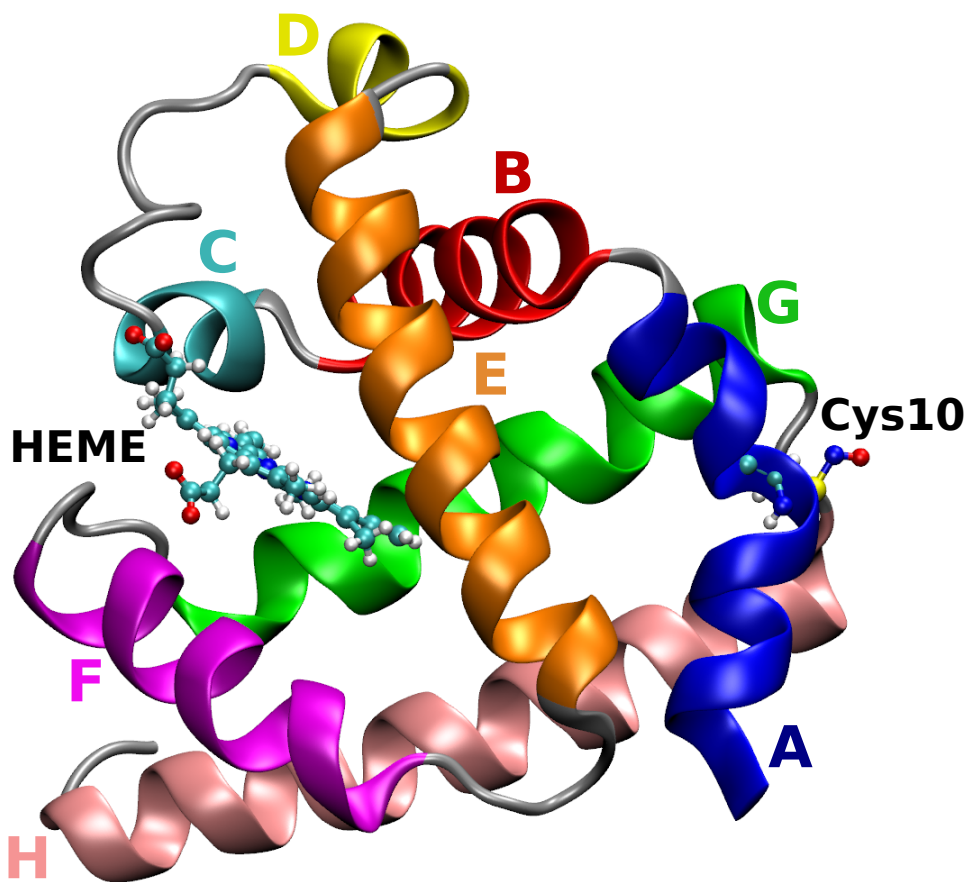


Figure 3: Structure of trans-MbSNO (Cartoon representation) with helices A to H in different color together with corresponding labels. The heme group and the S-Nitrosylated Cys10 residue are represented by CPK. Cys10 is part of the A-helix of Mb.

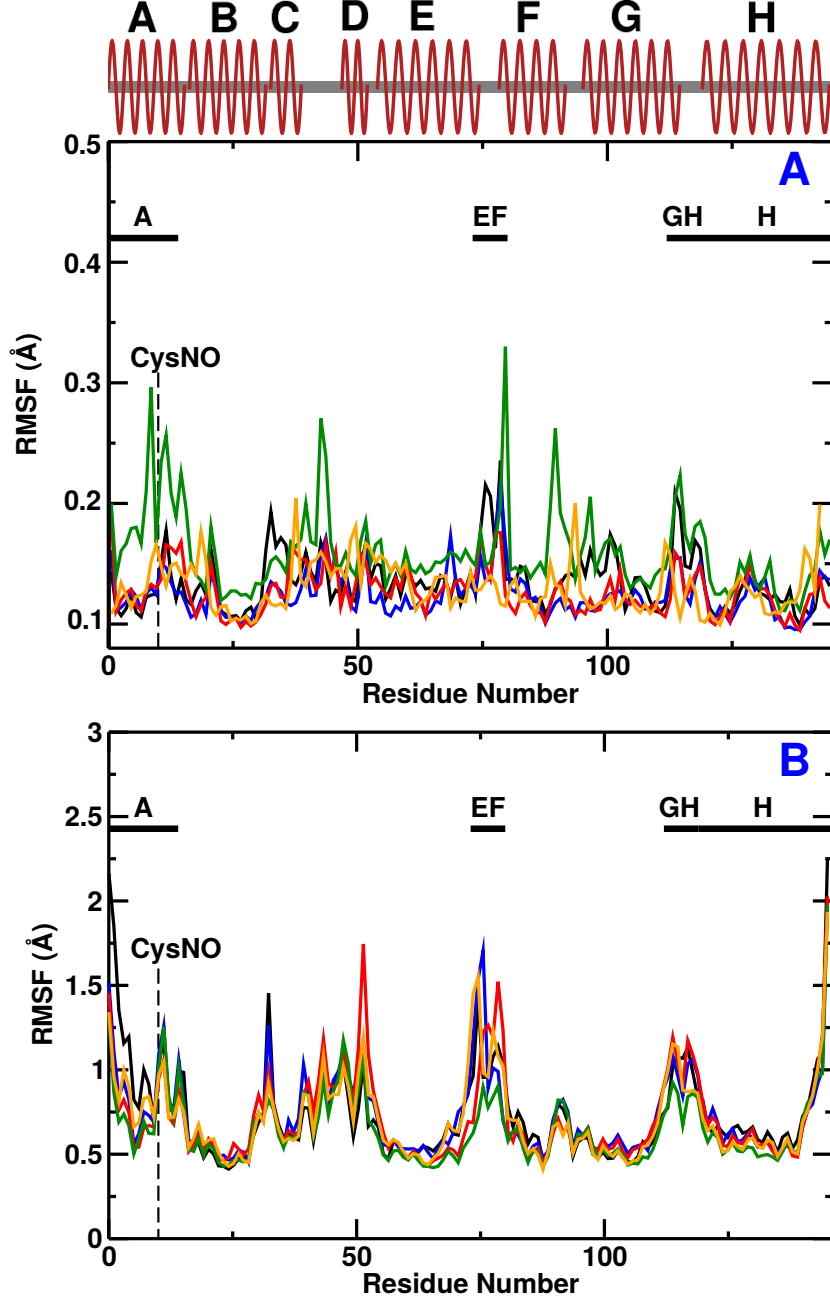


Figure 4: Root Mean Squared Fluctuation of each residue at 50 K (panel A) and 300 K (panel B) from simulations using the PC and MTP model. (Black line: WT, Red line: cis-MbSNO with PC, Blue line: trans-MbSNO with PC, Green line: cis-MbSNO with MTP and Orange line: trans-MbSNO with MTP). The location of CysNO (at position 10), and helix A (Ala2 to Glu15), helix H (Gly121 to Ser146), loop EF (Ala74 to Ile81) and loop GH (Glu113 to Gly120) are explicitly indicated. Note the different scales along the y -axis in panels A and B.

The root mean squared fluctuations of the C_{α} atoms of every residue at 50 K and 300 K from

10 ns simulations with the PC and MTP models are reported in Figure 4 (top and bottom) for the WT (black), cis-MbSNO (PC, red), trans-MbSNO (PC, blue), cis-MbSNO (MTP, green), and trans-MbSNO (MTP, orange). At 50 K all RMSFs are small and S-nitrosylation of Cys10 decreases the flexibility of cis- and trans-MbSNO with PC in the C-, E-, F-, and G-helix regions compared with WT. The RMSF for residues Lys31 to Glu35 (end of helix B and beginning of helix C) display reduced flexibility as a consequence of the chemical modification. The largest differences are found for the residues between Lys90 and Leu102 (end of helix F, FG loop, beginning of helix G). With MTPs on the -SNO label the RMSFs for cis-MbSNO are typically larger or equal compared with WT (PC) due to unfavorable conformation around the -SNO group whereas for trans-MbSNO they are comparable. Contrary to simulations at 50 K that sample the $C_\alpha C_\beta SN$ dihedral only at one particular angle, the dynamics of cis-MbSNO samples states characterized by angles of 94° and 80° (see blue line in Figure ??). The conformational change of S-nitrosylated Cys10 from 94° to 80° at such low temperature indicates an unfavorable conformation that could lead to a higher flexibility of the protein.

At 300 K, the differences in flexibility of each residue between WT, cis- and trans-MbSNO with both PC and MTP are much smaller. While the magnitude of the RMSF between 50 K and 300 K increases considerably, as expected, the differences between the systems become more specific. The flexibility of residues Ala2 to Cys10 (helix A) decreased with the modification in both cis- and trans-MbSNO compared to WT which indicates a rigidification of helix A and points to a clear impact of nitrosylation at Cys10 on the local dynamics of the protein. Moreover, increased flexibilities up to 1.7 \AA are found for residues Glu70 to Ile81 (EF loop). This is the region with the largest displacements in both, cis- and trans-MbSNO compared to WT.

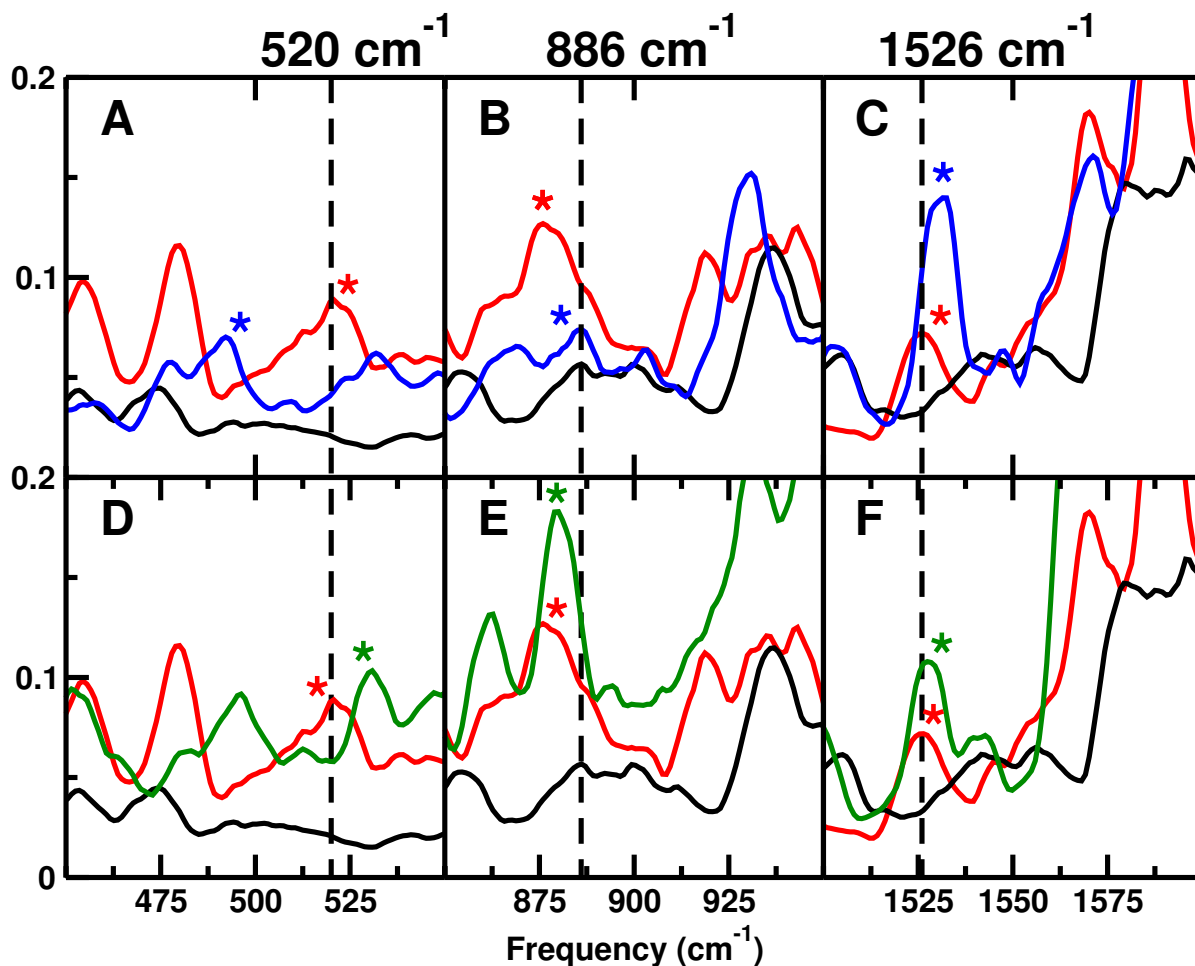


Figure 5: Comparison of the calculated IR spectra for WT, cis- and trans-MbSNO from 10 ns simulations at 50 K in the region of the SN stretch (panels A and D), SNO bend (panels B and E), and NO stretch (panels C and F). Top row from simulations with PC (black : WT, red : cis-MbSNO, blue : trans-MbSNO). Bottom row from simulations with PC and MTP (black : WT, red : cis-MbSNO with PC, green : cis-MbSNO with MTP). The dashed vertical lines indicate the experimental values of the corresponding vibrations in GSNO²⁸ and the colored stars label the spectral signatures to which the mode was assigned based on analysis of the power spectra. In general, the WT spectra (black) are featureless in the region where the -SNO label shows spectroscopic signatures.

The spectra related to the NO and SN stretches and the SNO bend are reported in Figures 5A to C from simulations for cis- and trans-SNO with PCs. A comparison for PC and MTP simulations is given in Figures 5D to F. For the NO stretch (Figure 5C) the peak for cis-MbSNO from simulations with PCs appears at 1526 cm⁻¹ compared with 1532 cm⁻¹ for trans-MbSNO. These absorption frequencies for the NO stretch compare with 1526 cm⁻¹

from experiments on GSNO in its solid state, i.e. identical to that for cis-MbSNO, and a blue shift of 6 cm^{-1} for trans-MbSNO between simulations and experiment. It is also noted that the NO-stretch vibration in CysNO (at 1538 cm^{-1} and 1540 cm^{-1} for cis- and trans-CysNO with MTPs) differs from that for cis-MbSNO and trans-MbSNO by 14 and 6 cm^{-1} , respectively, see Figure 2. Likewise, a blue-shift was observed for trans-CH₃SNO relative to cis-CH₃SNO for experiments in argon.³² The intensity of the NO band for trans-MbSNO is higher compared with that of cis-MbSNO. Figure 5C also shows that the NO stretch is clearly set apart from the nearby the amide-II band which is ranging from 1500 to 1620 cm^{-1} in the simulations and from 1500 to 1600 from experiments.⁶⁰ This should make it possible to locate the NO stretch mode from experiments, in particular when reference spectra for the WT protein or for two different isotopes of the label (¹⁴NO and ¹⁵NO) are subtracted.

The SN stretch and SNO bend modes are more challenging to identify for both conformations. The spectrum in Figure 5B has the SNO bending mode at 876 cm^{-1} for cis-MbSNO which shifts to 886 cm^{-1} for the trans-conformer. Finally, the SN stretch appears at 522 cm^{-1} for cis-MbSNO and at 494 cm^{-1} for the trans-conformer, see Figure 5A. Hence, the orientation of the NO group (cis vs. trans) shifts these modes by 6 to 28 cm^{-1} . Again, the magnitude of these shifts is consistent with the findings for CysNO in water.

In order to quantify the influence of the charge model used on the infrared signatures of the SN stretch, SNO bending, and the NO stretch, cis-MbSNO was considered. For this, a 10 ns MD simulation at 50 K was carried out with MTPs on the -SNO moiety. The corresponding spectra are shown in Figures 5D to F. The NO stretch from the simulations with MTP appears at 1527 cm^{-1} which is shifted by 1 cm^{-1} to the blue compared with the simulation with the PC model. The intensity of this peak increases considerably when using the more elaborate model for the electrostatics, see Figure 5F. For the SNO bending vibration the frequency maximum appears at 880 cm^{-1} in the simulation with MTPs which is a shift of 4

cm^{-1} to the blue compared with the PC simulation. Finally, the SN stretch is at 531 cm^{-1} , shifted by 9 cm^{-1} to the blue compared with the PC simulation. Hence, all three vibrations shift to the blue in simulations with the MTP model compared with PCs. Such shifts are typical for simulations with PCs and MTPs.^{61–65} The increased intensity with MTP model made it easier to detect the vibrations on the total IR spectrum of the protein, especially for SNO and NO.

In summary, it is noted that in the regions of the SN stretch, SNO bend and NO stretch modes the intensity of the spectrum for WT myoglobin (black trace in Figure ??) is characteristically low whereas those for the two nitrosylated variants show increased intensities (see arrows in Figure ??). The calculated IR spectra from simulations with PCs and the Fourier transform of the protein dipole autocorrelation function for WT, cis-MbSNO with PC and trans-MbSNO are reported in Figure ?. Spectral features of amide-I, amide-II and amide-III absorption bands are present in all spectra with varying intensities. Also, the blue shifted frequencies in particular for the NO-stretch vibration for trans- versus cis-SNO is consistent with experiments on model compounds in the gas phase or in argon matrices.

3.3 Water Structure and Global Structural Changes

Next, it is of interest to consider the local water ordering around the modification site (Cys10) for WT and nitrosylated Mb. The radial distribution function $g_{\text{S-OW}}(r)$ and corresponding coordination number $N_{\text{S-OW}}(r)$ of water oxygen (OW) with respect to the sulfur atom of Cys10 in WT, cis-MbSNO, and trans-MbSNO are shown in Figure 6. At 300 K and with PC for the simulations the first solvation shell peak appears at 3.5 \AA in all proteins. While the difference of the first solvation peak in terms of peak height and shape is marginal, the radial distribution functions for cis- and trans-MbSNO (red and blue) differ from that for WT (black) in the region between 4 \AA and 7.5 \AA , see Figure 6. It clearly shows that with

respect to the Cys10-sulfur atom both, cis-MbSNO and trans-MbSNO, are more highly solvated in the range of ~ 5 to 7 Å compared to WT. Since nitric oxide is more solvent exposed in trans-MbSNO (blue trace) compared to cis-MbSNO (red trace) the -SNO label is more highly hydrated in the trans-conformation. In terms of the overall hydration, the coordination number of WT and trans-MbSNO differs by 3 water molecules at a distance of 10 Å, see Figure 6, whereas WT and cis-MbSNO have the same overall hydration. Although the -SNO (modified Mb) group requires more space compared with -SH (WT Mb), attaching the -NO label recruits more water molecules. This is evidently an effect of the different electrostatics between water and the -SH and -SNO groups, respectively.

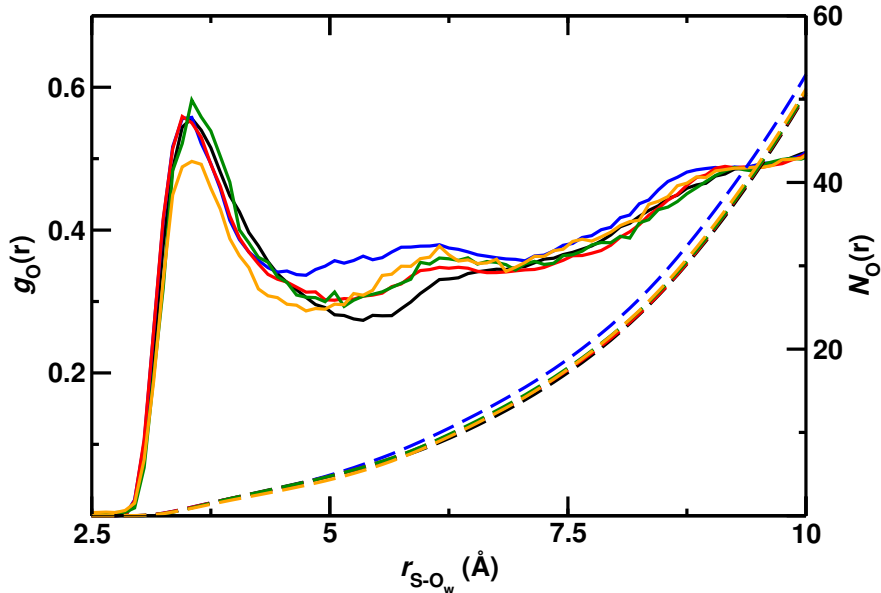


Figure 6: Radial distribution function of water oxygen and the corresponding coordination number of $N_O(r)$ of water oxygen with respect to the sulfur atom obtained from NVE simulations at 300 K. Color code: WT (black), cis-MbSNO with PC (red), trans-MbSNO with PC (blue), cis-MbSNO with MTP (green), trans-MbSNO with MTP (orange).

With the MTP model, trans-MbSNO displays a shallower first solvation shell compared to PC, while cis-MbSNO with MTP has comparable solvation to PC. The dissimilar impact of additional multipoles on the two conformers can be rationalized by the $\phi(\text{NC}_\alpha\text{C}_\beta\text{S})$ angles sampled during the dynamics. For cis-MbSNO and both charge models this an-

gle fluctuates around $\sim -60^\circ$ throughout the 10 ns simulation (see red and green lines in Figure ??B). However, for trans-MbSNO (see Figure ??B) the $\phi(\text{NC}_\alpha\text{C}_\beta\text{S})$ angle sampled differs between PC and MTP. With both models $\phi(\text{NC}_\alpha\text{C}_\beta\text{S})$ samples structures with $\sim -55^\circ$ - albeit only briefly for PCs - and $\sim 52^\circ$. For the simulation with PCs, in addition the orientation with $\phi(\text{NC}_\alpha\text{C}_\beta\text{S}) = -170^\circ$ is sampled. Also, the residence time in the conformation with $\phi(\text{NC}_\alpha\text{C}_\beta\text{S}) \sim -55^\circ$ differs between simulations with PC (9 ns) compared with MTP (5.75 ns) and the simulation with PCs spontaneously returns to the conformation with $\phi(\text{NC}_\alpha\text{C}_\beta\text{S}) = -62^\circ$. Consequently, the different level of solvent exposure can be the underlying reason for the shallower solvation shells observed with MTP. However, longer simulations (and hence more transitions) are required for quantitative characterizations of such residence times.

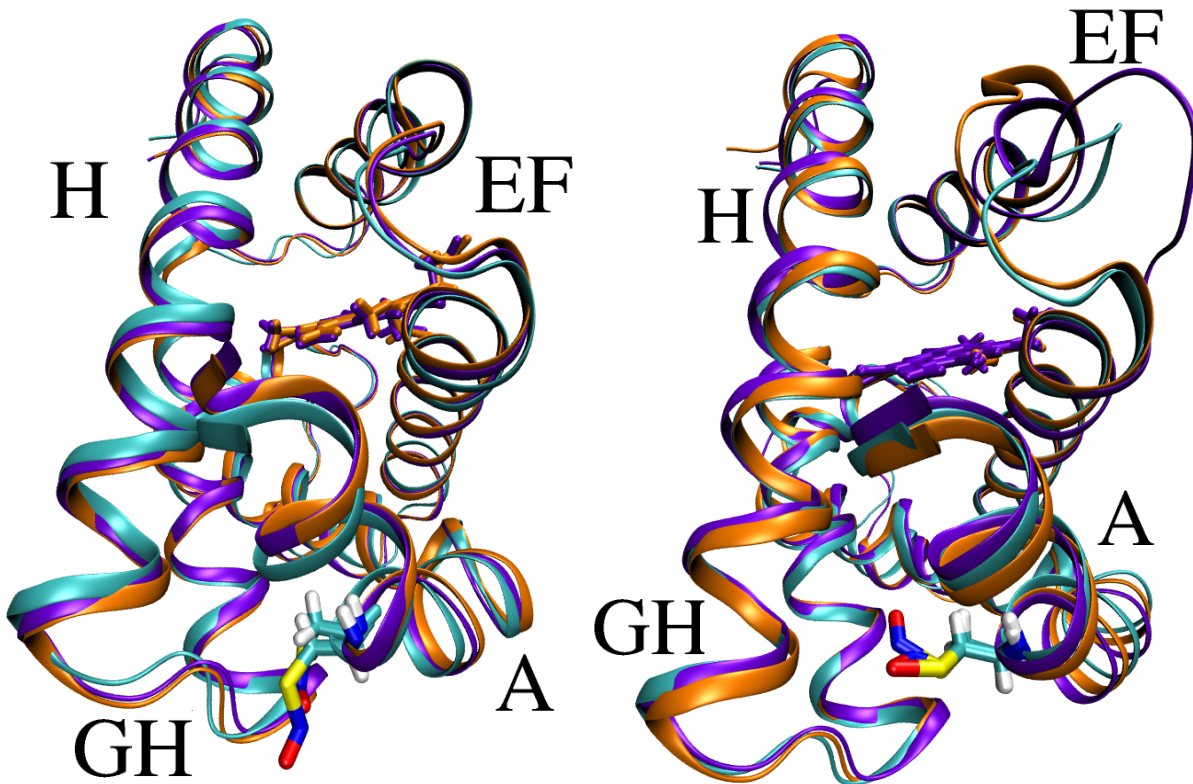


Figure 7: The conformational changes in the protein structure induced by S-Nitrosylation, averaged over the last ns of free dynamic simulations at 50 (Left) and 300 K (Right) with PC model. WT (cyan), cis-MbSNO (orange) and trans-MbSNO (violet). S-Nitrosylated Cys10 and the heme unit are represented by licorice. A, H helices and EF, GH loops are labeled.

Global Changes: For characterizing more global structural changes, the last nanosecond of the 10 ns production run have been analyzed to investigate the structural changes in the protein at 50 K and 300 K, respectively. The cis-MbSNO and trans-MbSNO structures are superimposed onto the WT simulation and the structures averaged over the last ns of the free dynamic simulations at 50 K (left) and 300 K (right) in Figure 7 for WT (cyan), cis-MbSNO (orange), and trans-MbSNO (violet), respectively. The dihedral angles $\phi(\text{C}_\beta\text{SNO})$ (for cis- versus trans-), $\phi(\text{C}_\alpha\text{C}_\beta\text{SN})$ and $\phi(\text{NC}_\alpha\text{C}_\beta\text{S})$ (for the position of the NO with respect to nearby loops and α -helices) determine the orientation of the -SNO label and reported in Figure ?? for 50 K and Figure ?? at 300 K. The time series show that all states sampled are also observed in the 2NRM X-ray structure.

Table 2: The average C_α RMSD (in Å) for Helix A, Helix H, Loop GH, Loop EF and the entire protein for cis-MbSNO and trans-MbSNO with respect to the WT X-Ray structure for the last nanosecond of a 10 ns free dynamics simulation at 50 and 300 K with PC and MTP models. As a comparison, the differences between the 2NRL and 2NRM structure are also given.

	50K				300K				X-Ray
	cis-MbSNO		trans-MbSNO		cis-MbSNO		trans-MbSNO		2NRM
	PC	MTP	PC	MTP	PC	MTP	PC	MTP	
Helix A	0.57	0.60	0.51	0.63	1.45	1.48	1.37	1.33	0.681
Helix H	0.86	1.67	1.00	1.01	1.19	1.19	1.11	0.86	0.627
Loop GH	1.31	0.71	0.68	0.93	1.72	1.68	1.55	1.92	1.076
loop EF	1.17	1.07	1.16	1.35	2.63	2.02	3.23	2.54	3.843
Protein	0.83	0.78	0.81	0.80	1.27	1.14	1.28	1.17	0.989

Although the entire protein structure is affected by the modification to a certain degree, four regions revealed most prominent changes. They are helix A (residues Ala2 to Glu15), helix H (residues Gly121 to Ser146), loop GH (residues Glu113 to Gly120), and loop EF (residues Ala74 to Ile81). The C_α RMSD of helix A, helix H, loop GH, loop EF and the entire protein for cis- and trans-MbSNO with respect to the WT X-ray structure during the last nanosecond of the 10 ns free dynamics simulations are summarized in Table 2.

At 50 K, the C_α RMSD for [cis-MbSNO, trans-MbSNO] compared to X-Ray WT are [0.83, 0.81] Å with PC and [0.78, 0.80] Å with MTP, respectively, which signals good preservation of the overall structure for the methods chosen. The C_α RMSD calculated between the 2NRL and 2NRM structures is 0.99 Å which is compatible with the C_α RMSD calculated from the simulations with both, PC and MTP electrostatic models for the NO-label. These results show that the orientation of nitric oxide has a limited effect on the overall structure of the protein with only 0.02 Å difference between the two conformers with both charge models. Further, the same trend is observed in the local dynamics of the helices. C_α RMSD values of the individual helices (A and H) deviate by 0.06 Å to 0.14 Å for cis-MbSNO compared to trans-MbSNO with PC, respectively. These small but consistent differences in the RMSD values between the two conformers can be rationalized by the orientation of nitric oxide with respect to $\phi(C_\beta\text{SNO})$ which is 0° in cis-MbSNO and 180° in trans-MbSNO.

At 300 K, the C_α RMSD of the cis-MbSNO and trans-MbSNO with respect to the WT X-Ray structure are 1.27 Å, 1.28 Å with PC and 1.14 Å, 1.17 Å with MTP, respectively. The local motion of the protein causes larger C_α RMSD values of helix A in both, trans-MbSNO with PC and cis-MbSNO with PC. The values, with respect to X-Ray WT structure, were 1.45 Å and 1.37 Å respectively. The C_α RMSD of helix H and loop GH were 1.19 and 1.72 Å in cis-MbSNO with PC, compared with 1.11 and 1.55 Å in trans-MbSNO with PC. Furthermore, the largest deviation from the X-Ray WT structure is observed for the EF loop, see Table 2. The relatively flexible loop moved closer to helix H in cis-MbSNO. Contrary to that, the movement of the loop was in the opposite direction for trans-MbSNO with PC. The C_α RMSD of loop EF is 2.63 Å in cis-MbSNO with PC and 3.23 Å in trans-MbSNO with PC.

Depending on the orientation of the -SNO group (cis or trans), additional contacts with the protein can emerge. At 50 K, the $\phi(C_\alpha C_\beta\text{SN})$ angles sampled for cis- and trans-MbSNO

are shown in Figure ?? . For cis-MbSNO the -SNO group is closer to the GH loop than for trans-MbSNO. Consequently, nitrosylation of Cys10 in its cis-conformer will lead to steric hindrance with the GH loop and pushes it away from its position in WT Mb to avoid overlap between Leu117 and Cys10. Concomitantly, helix A (containing residue Cys10) is forced in the opposite direction of loop GH. Finally, helix H can push into the void created by the movement of helix A. This same steric hindrance was present to a lesser extent for trans-MbSNO and WT. The movement of the EF loop is also visible in Figure 7. The loop had a C_α RMSD of 1.17 Å in cis-MbSNO and 1.16 Å in trans-MbSNO. The resulting crowding involving residues Cys10 and Leu117 without concomitant motion of loop GH and helix A upon nitrosylation is shown in Figure 8.

At 300 K, the influence of the NO-modification on the structure of Mb is more pronounced than for 50 K, specifically for loop EF. However, the similar C_α RMSD for cis- and trans-MbSNO with respect to WT (see Table 2) shows that the orientation of the nitric oxide has only a limited effect on the overall structure of the protein. In the conformation with $\phi(C_\alpha C_\beta SN) \sim -85^\circ$ (for cis-MbSNO with PC (red) and trans-MbSNO with MTP (orange), see Figure ??A) the nitric oxide group resides midway between loop GH and helix A. The conformational transition to $\phi(C_\alpha C_\beta SN) \sim 160^\circ$ moves the -NO group closer to helix H. For cis-MbSNO with MTPs (green) this is the only state sampled throughout the simulation and corresponds to the major component observed in the 2NRM X-ray structure. For cis-MbSNO with PCs (red) there is a spontaneous transition between the minor and the major conformer. This suggests that the major conformer is probably lower in energy but for a firm conclusion on this considerably more extended simulations are required.

For trans-MbSNO (blue and orange traces in Figure ??A) four metastable states for the orientation of $\phi(C_\alpha C_\beta SN)$ were found in simulations with PCs. The orientation with $\phi(C_\alpha C_\beta SN) \sim 155^\circ$ is prevalent (Figure ??A). In this conformation the NO modification faces towards he-

lix A. After 1 ns, a transition to $\phi(C_\alpha C_\beta SN) \sim 52^\circ$ occurs. Concomitantly, the $\phi(NC_\alpha C_\beta S)$ dihedral changes from ~ -55 to $\sim -180^\circ$ (Figure ??B) which positions the nitric oxide towards the GH loop. A next transition leads to $\phi(C_\alpha C_\beta SN) \sim -70^\circ$ with the NO midway between loop GH and helix A, as was found for cis-MbSNO. Finally, a transition to a state with $\phi(NC_\alpha C_\beta S) \sim 55^\circ$, and $\phi(C_\alpha C_\beta SN) \sim 95^\circ$ occurred in which the NO faced towards the inner part of the protein. One should note that this was the only occasion on which SNO was buried into the protein. This conformation reduces the probability for the solvent accessibility of SNO.

S-nitrosylation-induced structural changes have also been reported for the crystal structures of the WT (2NRL) and cis-MbSNO (2NRM). This is exacerbated by the high C_α RMSD of loop EF as was observed in the present simulations (see Table 2). X-ray experiments revealed that the CysNO can induce crowding between Leu117 (loop GH) and Ala6 (helix A) if these parts of the protein structure did not move⁵² which also been observed in the simulation of cis-MbSNO. The distance between the C_α atoms of Cys10 and Leu117 (r_{10-117}) in the X-Ray structure is 5.97 Å (for 2NRL, WT) and 6.35 Å (for the major conformer of 2NRM). This compares with an averaged r_{10-117} of 6.18 Å for WT (black trace in Figure ??) and 7.39 for cis-MbSNO with PC (red trace in Figure ??) in the simulations. The same simulation for cis-MbSNO with MTP leads to relaxation of the structure after ~ 2 ns (green trace in Figure ??). Finally, restarting the cis-MbSNO simulation with PC after 10 ns but with MTPs on the -SNO group also leads to relaxation towards the value from the X-ray structure. So, with MTP model, r_{10-117} assumed the value found in X-Ray whereas with PC it does not. This finding shows that repositioning of loop GH and helix A occurs to accommodate residues Cys10 and Leu117 in cis-MbSNO. The effect is demonstrated in Figure 8. Although the averaged r_{10-117} decreases to 6.37 Å for cis-MbSNO with MTP, the steric overlap is prevented due to sampling the $\phi(C_\alpha C_\beta SN)$ dihedral at different angles (85° and 94°) than cis-MbSNO with PC (red in Figure ??). Quantum chemical calculations indicate

that the potential energy curve along the CCSN dihedral is flat between 50° and 300° with minima at 100° and 250° and a barrier between them of 2 kcal/mol at the MP2 level of theory.

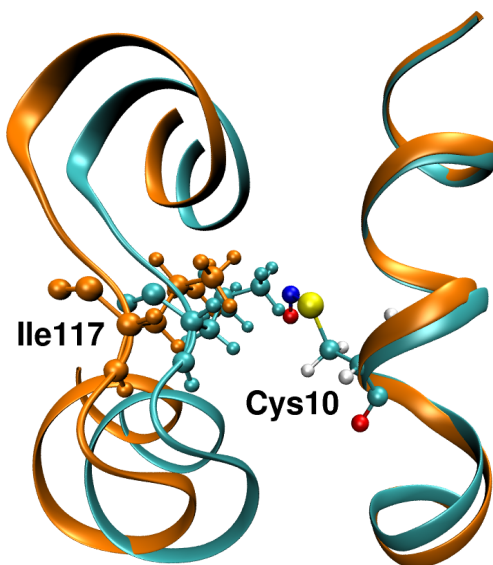


Figure 8: CPK representation of S-nitrosylated Cys10 and Leu117 (labelled) which demonstrates the crowding that would occur if there was no helix movement in cis-MbSNO. The WT and cis-MbSNO structures are shown by cyan and orange cartoon representations, respectively.

The structural changes induced by nitrosylation at Cys10 also influence local hydration between the helix A, helix H and loop GH, see Figure ?? . The chemical modification leads to a decrease of hydration in this region by 30 % between the WT and trans-MbSNO. Given the prominent role that water molecules can play in protein folding,⁶⁶ and for function,^{67,68} such a change in hydration may also be functionally relevant for a PTM such as nitrosylation. Also, the degree of hydration may affect the stability of the protein as has recently been demonstrated for insulin dimer. Mutation of residue PheB24 to Ala or Gly leads to water influx and destabilization of the dimer by a factor of 2 to 3.^{69–73}

4 Conclusion

The present work reported on the structural, dynamical and spectroscopic implications of nitrosylation at cysteine. For this, CysNO as a model and nitrosylated Mb (MbSNO) were considered. For both systems it was found that cis- and trans-orientations can be spectroscopically distinguished. While for CysNO the spectroscopic signatures can be more readily differentiated from other vibrational modes this is more challenging for MbSNO due to the larger number of vibrations and overlap with other vibrational excitations. Nevertheless, the spectroscopic signatures can be clearly located with both, simulations using PC and MTP models, see Figure 5. From recording and subtracting the IR spectrum for WT Mb, or the difference spectrum between MbS¹⁴NO and MbS¹⁵NO (as for MbNO²⁹) it should be possible to identify the IR signatures for nitrosylation in all proteins under physiological conditions for which such experiments are possible.

One consequence of nitrosylation is that local hydration changes around the modification site compared with the WT protein and different hydration between the A- and H-helices. For the protein considered here, myoglobin, 3 more water molecules were found to be recruited for -SNO compared with -SH for modification at Cys10. Although this number may appear small, given the functional role of individual, local water molecules that has been established in other proteins, this observation may still be functionally relevant. Furthermore, S-nitrosylation leads to discernible spectroscopic features in the infrared spectrum of MbSNO and to structural changes near the modification site.

It is also of interest to note that for nitrosylated Cysteine cis- and trans-orientations have been observed experimentally in human thioredoxin at position Cys69.⁷⁴ Also, the nitrosylated Cys62 was completely buried and points towards the protein interior which was also found for a short time during the present simulations for the trans-conformer.

In summary, S-nitrosylation in myoglobin was found to lead to detectable spectroscopic features in the infrared. Local hydration is enhanced as a consequence of the modification and the structure and dynamics at distant sites in the protein can be changed appreciably and are consistent with X-ray experiments.

5 Acknowledgment

This work was supported by the Swiss National Science Foundation grants 200021-117810, 200020-188724, the NCCR MUST, and the University of Basel which is gratefully acknowledged.

References

- (1) Sessa, W. C. The nitric oxide synthase family of proteins. *J. Vasc. Res.* **1994**, *31*, 131–143.
- (2) Houk, K.; Hietbrink, B. N.; Bartberger, M. D.; McCarren, P. R.; Choi, B. Y.; Voyksner, R. D.; Stamler, J. S.; Toone, E. J. Nitroxyl disulfides, novel intermediates in transnitrosation reactions. *J. Am. Chem. Soc.* **2003**, *125*, 6972–6976.
- (3) Kone, B. C.; Kuncewicz, T.; Zhang, W.; Yu, Z.-Y. Protein interactions with nitric oxide synthases: controlling the right time, the right place, and the right amount of nitric oxide. *Am. J. Physiol. Renal. Physiol.* **2003**, *285*, F178–F190.
- (4) Cooper, C. E. Nitric oxide and iron proteins. *Biochim. Biophys. Acta* **1999**, *1411*, 290–309.
- (5) Russwurm, M.; Koesling, D. NO activation of guanylyl cyclase. *EMBO. J.* **2004**, *23*, 4443–4450.

- (6) Astier, J.; Lindermayr, C. Nitric oxide-dependent posttranslational modification in plants: an update. *Int. J. Mol. Sci.* **2012**, *13*, 15193–15208.
- (7) Hess, D. T.; Stamler, J. S. Regulation by S-nitrosylation of protein post-translational modification. *J. Biol. Chem.* **2012**, *287*, 4411–4418.
- (8) Sun, J.; Steenbergen, C.; Murphy, E. S-nitrosylation: NO-related redox signaling to protect against oxidative stress. *Antioxid. Redox Signal.* **2006**, *8*, 1693–1705.
- (9) Hess, D. T.; Matsumoto, A.; Kim, S.-O.; Marshall, H. E.; Stamler, J. S. Protein S-nitrosylation: purview and parameters. *Nat. Rev. Mol. Cell Biol.* **2005**, *6*, 150.
- (10) Yasukawa, T.; Tokunaga, E.; Ota, H.; Sugita, H.; Martyn, J. J.; Kaneki, M. S-nitrosylation-dependent inactivation of Akt/protein kinase B in insulin resistance. *J. Biol. Chem.* **2005**, *280*, 7511–7518.
- (11) Wu, M.; Katta, A.; Gadde, M. K.; Liu, H.; Kakarla, S. K.; Fannin, J.; Paturi, S.; Arvapalli, R. K.; Rice, K. M.; Wang, Y. et al. Aging-associated dysfunction of Akt/protein kinase B: S-nitrosylation and acetaminophen intervention. *PLoS One* **2009**, *4*, e6430.
- (12) Chen, Y.-Y.; Chu, H.-M.; Pan, K.-T.; Teng, C.-H.; Wang, D.-L.; Wang, A. H.-J.; Khoo, K.-H.; Meng, T.-C. Cysteine S-nitrosylation protects protein-tyrosine phosphatase 1B against oxidation-induced permanent inactivation. *J. Biol. Chem.* **2008**, *283*, 35265–35272.
- (13) Barrett, D. M.; Black, S. M.; Todor, H.; Schmidt-Ullrich, R. K.; Dawson, K. S.; Mikkelsen, R. B. Inhibition of protein-tyrosine phosphatases by mild oxidative stresses is dependent on S-nitrosylation. *J. Biol. Chem.* **2005**, *280*, 14453–14461.
- (14) Zhou, C.; Liang, J.; Cheng, S.; Shi, T.; Houk, K.; Wei, D.-Q.; Zhao, Y.-L. Ab initio molecular metadynamics simulation for S-nitrosylation by nitric oxide: S-nitroxide as the key intermediate. *Mol. Simul.* **2017**, *43*, 1134–1141.

- (15) Gow, A. J.; Buerk, D. G.; Ischiropoulos, H. A novel reaction mechanism for the formation of S-nitrosothiol in vivo. *J. Biol. Chem.* **1997**, *272*, 2841–2845.
- (16) Martinez-Ruiz, A.; Araújo, I. M.; Izquierdo-Alvarez, A.; Hernansanz-Agustin, P.; Lamas, S.; Serrador, J. M. Specificity in S-nitrosylation: a short-range mechanism for NO signaling? *Antioxid. Redox Signal.* **2013**, *19*, 1220–1235.
- (17) Foster, M. W.; McMahon, T. J.; Stamler, J. S. S-nitrosylation in health and disease. *Trends Mol. Med.* **2003**, *9*, 160–168.
- (18) Jaffrey, S. R.; Erdjument-Bromage, H.; Ferris, C. D.; Tempst, P.; Snyder, S. H. Protein S-nitrosylation: a physiological signal for neuronal nitric oxide. *Nat. Cell Biol.* **2001**, *3*, 193–197.
- (19) Camerini, S.; Polci, M. L.; Restuccia, U.; Usuelli, V.; Malgaroli, A.; Bachi, A. A novel approach to identify proteins modified by nitric oxide: the HIS-TAG switch method. *J. Proteome Res.* **2007**, *6*, 3224–3231.
- (20) Shao, S.; Chen, B.; Cheng, J.; Wang, C.; Zhang, Y.; Shao, L.; Hu, Y.; Han, Y.; Han, F.; Li, X. A fluorogenic probe for imaging protein S-nitrosylation in live cells. *Biosens. Bioelectron.* **2017**, *94*, 162–168.
- (21) Wang, H.; Xian, M. Chemical methods to detect S-nitrosation. *Curr. Opin. Chem. Biol.* **2011**, *15*, 32–37.
- (22) Alcock, L. J.; Perkins, M. V.; Chalker, J. M. Chemical methods for mapping cysteine oxidation. *Chem. Soc. Rev.* **2018**, *47*, 231–268.
- (23) Paulsen, C. E.; Carroll, K. S. Cysteine-mediated redox signaling: chemistry, biology, and tools for discovery. *Chem. Rev.* **2013**, *113*, 4633–4679.
- (24) Devarie-Baez, N. O.; Zhang, D.; Li, S.; Whorton, A. R.; Xian, M. Direct methods for detection of protein S-nitrosylation. *Methods* **2013**, *62*, 171–176.

- (25) Forrester, M. T.; Foster, M. W.; Benhar, M.; Stamler, J. S. Detection of protein S-nitrosylation with the biotin-switch technique. *Free Radic. Biol. Med.* **2009**, *46*, 119–126.
- (26) Koziol, K. L.; Johnson, P. J.; Stucki-Buchli, B.; Waldauer, S. A.; Hamm, P. Fast infrared spectroscopy of protein dynamics: advancing sensitivity and selectivity. *Curr. Opin. Struc. Biol.* **2015**, *34*, 1–6.
- (27) Hamm, P.; Zanni, M. *Concepts and Methods of 2D Infrared Spectroscopy*; Cambridge University Press, 2011.
- (28) Walsh, G. M.; Leane, D.; Moran, N.; Keyes, T. E.; Forster, R. J.; Kenny, D.; O'Neill, S. S-Nitrosylation of platelet $\alpha\text{IIb}\beta 3$ as revealed by raman spectroscopy. *Biochem.* **2007**, *46*, 6429–6436.
- (29) Coyle, C. M.; Vogel, K. M.; Rush III, T. S.; and R. Williams, P. M. K.; Spiro, T. G.; Dou, Y.; Ikeda-Saito, M.; Olson, J. S.; Zgierski, M. Z. *Biochem.* **2003**, *42*, 4896.
- (30) Manning, M. C. Use of infrared spectroscopy to monitor protein structure and stability. *Expert Rev. Proteomic* **2005**, *2*, 731–743.
- (31) Kramer, R. M.; Shende, V. R.; Motl, N.; Pace, C. N.; Scholtz, J. M. Toward a molecular understanding of protein solubility: increased negative surface charge correlates with increased solubility. *Biophys. J* **2012**, *102*, 1907–1915.
- (32) Mueller, R.; Huber, J. R. Two rotational isomers of methyl thionitrite: light-induced, reversible isomerization in an argon matrix. *J. Phys. Chem.* **1984**, *88*, 1605–1608.
- (33) Canneva, A.; Della Vedova, C. O.; Mitzel, N. W.; Erben, M. F. Conformational properties of ethyl-and 2, 2, 2-trifluoroethyl thionitrites, (CX₃CH₂SNO, X= H and F). *J. Phys. Chem. A* **2015**, *119*, 1524–1533.

- (34) Gregori, B.; Guidoni, L.; Chiavarino, B.; Scuderi, D.; Nicol, E.; Frison, G.; Fornarini, S.; Crestoni, M. E. Vibrational signatures of S-nitrosoglutathione as gaseous, protonated species. *J. Phys. Chem. B* **2014**, *118*, 12371–12382.
- (35) Bartberger, M. D.; Houk, K.; Powell, S. C.; Mannion, J. D.; Lo, K. Y.; Stamler, J. S.; Toone, E. J. Theory, spectroscopy, and crystallographic analysis of S-nitrosothiols: conformational distribution dictates spectroscopic behavior. *J. Am. Chem. Soc.* **2000**, *122*, 5889–5890.
- (36) Romeo, A. A.; Filosa, A.; Capobianco, J. A.; English, A. M. Metal chelators inhibit S-nitrosation of Cys β 93 in oxyhemoglobin. *J. Am. Chem. Soc.* **2001**, *123*, 1782–1783.
- (37) Hess, D. T.; Matsumoto, A.; Nudelman, R.; Stamler, J. S. S-nitrosylation: spectrum and specificity. *Nat. Cell Biol.* **2001**, *3*, E46–E48.
- (38) Khomyakov, D. G.; Timerghazin, Q. K. Toward reliable modeling of S-nitrosothiol chemistry: Structure and properties of methyl thionitrite (CH₃SNO), an S-nitrosocysteine model. *J. Chem. Phys.* **2017**, *147*, 044305.
- (39) Timerghazin, Q. K.; Peslherbe, G. H.; English, A. M. Structure and stability of HSNO, the simplest S-nitrosothiol. *Phys. Chem. Chem. Phys.* **2008**, *10*, 1532–1539.
- (40) Bignon, E.; Allega, M. F.; Lucchetta, M.; Tiberti, M.; Papaleo, E. Computational structural biology of S-nitrosylation of cancer targets. *Front. Oncol.* **2018**, *8*, 272.
- (41) Melvin, A. C.; Jones, W. M.; Lutzke, A.; Allison, C. L.; Reynolds, M. M. S-Nitrosoglutathione exhibits greater stability than S-nitroso-N-acetylpenicillamine under common laboratory conditions: A comparative stability study. *Nitric Oxide* **2019**, *92*, 18–25.
- (42) El Hage, K.; Brickel, S.; Hermelin, S.; Gaulier, G.; Schmidt, C.; Bonacina, L.; van

- Keulen, S. C.; Bhattacharyya, S.; Chergui, M.; Hamm, P. et al. Implications of Short Time Scale Dynamics on Long Time Processes. *Struct. Dyn.* **2017**, *4*, 061507.
- (43) Han, S. Force field parameters for S-nitrosocysteine and molecular dynamics simulations of S-nitrosated thioredoxin. *Biochem. Biophys. Res. Commun.* **2008**, *377*, 612–616.
- (44) Petrov, D.; Margreitter, C.; Grandits, M.; Oostenbrink, C.; Zagrovic, B. A systematic framework for molecular dynamics simulations of protein post-translational modifications. *PLoS Comput Biol* **2013**, *9*, e1003154.
- (45) Brooks, B. R.; Brooks, C. L., III; Mackerell, A. D., Jr.; Nilsson, L.; Petrella, R. J.; Roux, B.; Won, Y.; Archontis, G.; Bartels, C.; Boresch, S. et al. CHARMM: The Biomolecular Simulation Program. *J. Comput. Chem.* **2009**, *30*, 1545–1614.
- (46) Huang, J.; MacKerell Jr, A. D. CHARMM36 all-atom additive protein force field: Validation based on comparison to NMR data. *J. Comput. Chem.* **2013**, *34*, 2135–2145.
- (47) Hairer, E.; Lubich, C.; Wanner, G. Geometric numerical integration illustrated by the Störmer–Verlet method. *Acta Numer.* **2003**, *12*, 399–450.
- (48) Ryckaert, J.-P.; Ciccotti, G.; Berendsen, H. J. Numerical integration of the cartesian equations of motion of a system with constraints: molecular dynamics of n-alkanes. *J. Comput. Phys.* **1977**, *23*, 327–341.
- (49) Steinbach, P. J.; Brooks, B. R. New spherical-cutoff methods for long-range forces in macromolecular simulation. *J. Comput. Chem.* **1994**, *15*, 667–683.
- (50) Darden, T.; York, D.; Pedersen, L. Particle mesh Ewald: An $N\log(N)$ method for Ewald sums in large systems. *J. Chem. Phys.* **1993**, *98*, 10089–10092.
- (51) Jorgensen, W. L.; Chandrasekhar, J.; Madura, J. D.; Impey, R. W.; Klein, M. L.

- Comparison of simple potential functions for simulating liquid water. *J. Chem. Phys.* **1983**, *79*, 926–935.
- (52) Schreiter, E. R.; Rodríguez, M. M.; Weichsel, A.; Montfort, W. R.; Bonaventura, J. S-nitrosylation-induced conformational change in blackfin tuna myoglobin. *J. Biol. Chem.* **2007**, *282*, 19773–19780.
- (53) Head-Gordon, M.; Pople, J. A.; Frisch, M. J. MP2 energy evaluation by direct methods. *Chem. Phys. Lett.* **1988**, *153*, 503–506.
- (54) Kendall, R. A.; Dunning Jr, T. H.; Harrison, R. J. Electron affinities of the first-row atoms revisited. Systematic basis sets and wave functions. *J. Chem. Phys.* **1992**, *96*, 6796–6806.
- (55) Frisch, M. J.; Trucks, G. W.; Schlegel, H. B.; Scuseria, G. E.; Robb, M. A.; Cheeseman, J. R.; Scalmani, G.; Barone, V.; Mennucci, B.; Petersson, G. A. et al. Gaussian09 Revision D.01. Gaussian Inc. Wallingford CT 2009.
- (56) Kramer, C.; Gedeck, P.; Meuwly, M. Atomic multipoles: Electrostatic potential fit, local reference axis systems, and conformational dependence. *J. Comput. Chem.* **2012**, *33*, 1673–1688.
- (57) Bereau, T.; Kramer, C.; Monnard, F. W.; Nogueira, E. S.; Ward, T. R.; Meuwly, M. Scoring multipole electrostatics in condensed-phase atomistic simulations. *J. Phys. Chem. B* **2013**, *117*, 5460–5471.
- (58) Hedin, F.; El Hage, K.; Meuwly, M. A toolkit to fit nonbonded parameters from and for condensed phase simulations. *J. Chem. Inf. Model.* **2016**, *56*, 1479–1489.
- (59) Lammers, S.; Meuwly, M. Investigating the relationship between infrared spectra of shared protons in different chemical environments: A comparison of protonated diglyme and protonated water dimer. *J. Phys. Chem. A* **2007**, *111*, 1638–1647.

- (60) van de Weert, M.; Haris, P. I.; Hennink, W. E.; Crommelin, D. J. Fourier transform infrared spectrometric analysis of protein conformation: effect of sampling method and stress factors. *Anal. Biochem.* **2001**, *297*, 160–169.
- (61) Nutt, D.; Meuwly, M. Theoretical investigation of infrared spectra and pocket dynamics of photodissociated carbonmonoxy myoglobin. *Biophys. J.* **2003**, *85*, 3612–3623.
- (62) Devereux, M.; Plattner, N.; Meuwly, M. Application of Multipolar Charge Models and Molecular Dynamics Simulations to Study Stark Shifts in Inhomogeneous Electric Fields. *J. Phys. Chem. A* **2009**, *113*, 13199–13209.
- (63) Plattner, N.; Meuwly, M. Higher order multipole moments for molecular dynamics simulations. *J. Mol. Model.* **2009**, *15*, 687–694.
- (64) Plattner, N.; Meuwly, M. Atomistic simulations of CO vibrations in ices relevant to astrochemistry. *ChemPhysChem* **2008**, *9*, 1271–1277.
- (65) Plattner, N.; Meuwly, M. The role of higher CO-multipole moments in understanding the dynamics of photodissociated carbonmonoxide in myoglobin. *Biophys. J.* **2008**, *94*, 2505–2515.
- (66) Schiro, G.; Fichou, Y.; Gallat, F.-X.; Wood, K.; Gabel, F.; Moulin, M.; Haertlein, M.; Heyden, M.; Colletier, J.-P.; Orecchini, A. et al. Translational diffusion of hydration water correlates with functional motions in folded and intrinsically disordered proteins. *Nat. Chem.* **2015**, *6*, 1–8.
- (67) Pocker, Y. Water in enzyme reactions: biophysical aspects of hydration-dehydration processes. *Cell. Mol. Life Sci.* **2000**, *57*, 1008–1017.
- (68) Pal, S.; Zewail, A. Dynamics of water in biological recognition. *Chem. Rev.* **2004**, *104*, 2099–2123.

- (69) Strazza, S.; Hunter, R.; Walker, E.; Darnall, D. W. The thermodynamics of bovine and porcine insulin and proinsulin association determined by concentration difference spectroscopy. *Arch. Biochem. Biophys.* **1985**, *238*, 30–42.
- (70) Desmond, J. L.; Koner, D.; Meuwly, M. Probing the Differential Dynamics of the Monomeric and Dimeric Insulin from Amide-I IR Spectroscopy. *J. Phys. Chem. B* **2019**, *123*, 6588–6598.
- (71) Raghunathan, S.; El Hage, K.; Desmond, J. L.; Zhang, L.; Meuwly, M. The Role of Water in the Stability of Wild-type and Mutant Insulin Dimers. *J. Phys. Chem. B* **2018**, *122*, 7038–7048.
- (72) Zoete, V.; Meuwly, M.; Karplus, M. Study of the insulin dimerization: Binding free energy calculations and per-residue free energy decomposition. *Proteins: Structure, Function, and Bioinformatics* **2005**, *61*, 79–93.
- (73) Zoete, V.; Meuwly, M.; Karplus, M. A comparison of the dynamic behavior of monomeric and dimeric insulin shows structural rearrangements in the active monomer. *J. Mol. Biol.* **2004**, *342*, 913–929.
- (74) Weichsel, A.; Brailey, J. L.; Montfort, W. R. Buried S-nitrosocysteine revealed in crystal structures of human thioredoxin. *Biochem.* **2007**, *46*, 1219–1227.

The Effects of S-Nitrosylation on the Conformational Dynamics of Myoglobin

Haydar Taylan Turan¹ and Markus Meuwly^{1*}

¹*Department of Chemistry, University of Basel, Klingelbergstrasse 80, Basel, Switzerland*

E-mail: m.meuwly@unibas.ch

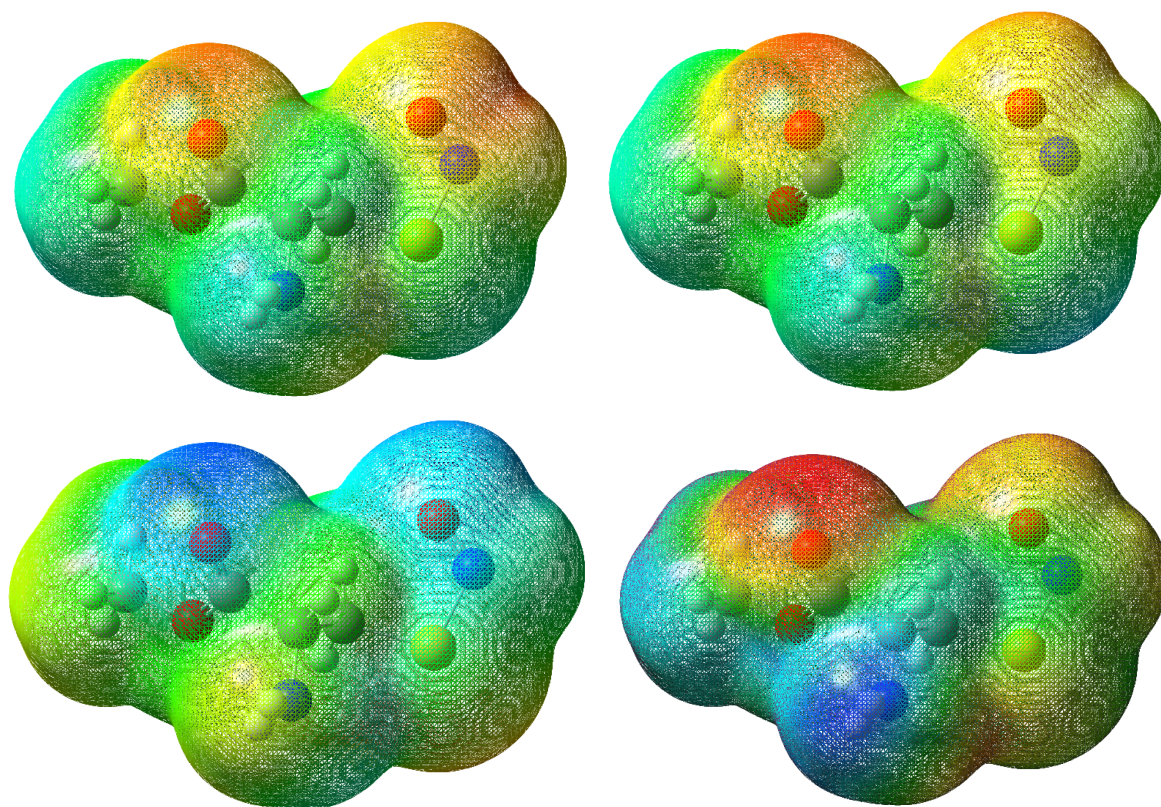


Figure S1: The density cube generated from the cis-CysNO residue with PC model (Up-Left) and MTP model (Up-Right). The cube generated from the difference between PC and MTP model (Down-Left) and reference ESP cube at MP2/aug-cc-pVDZ level (Down-Right).

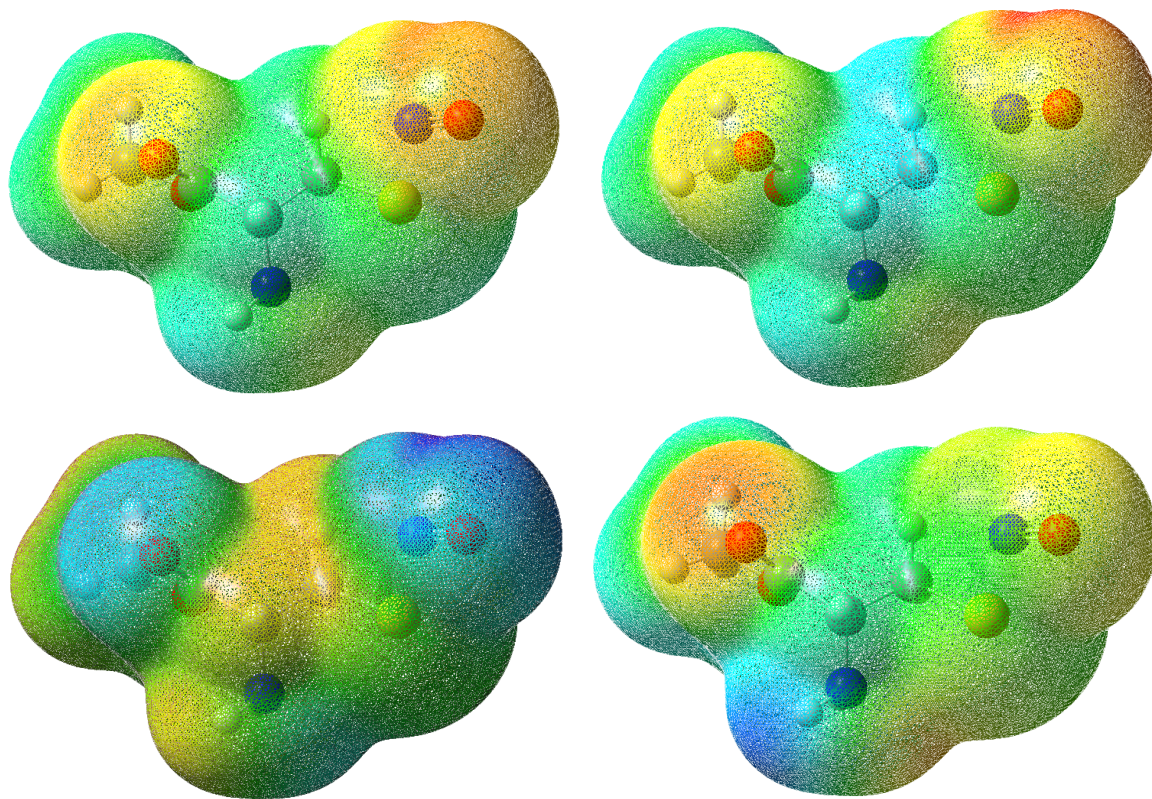


Figure S2: The density cube generated from the trans-CysNO residue with PC model (Up-Left) and MTP model (Up-Right). The cube generated from the difference between PC and MTP model (Down-Left) and reference ESP cube at MP2/aug-cc-pVDZ level (Down-Right).

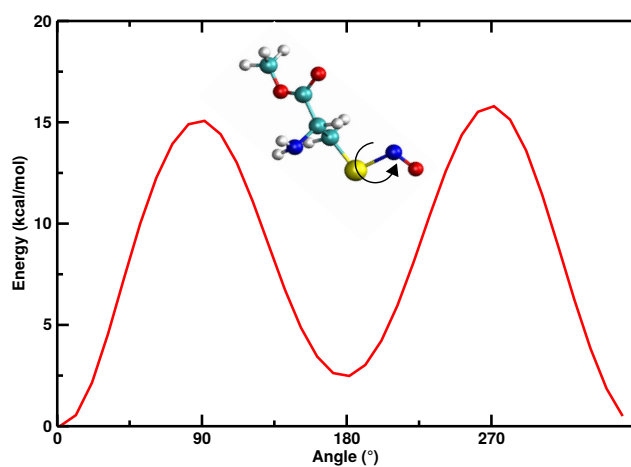


Figure S3: The energy profile of the CSNO torsion angle at the MP2/aug-cc-pVDZ level of theory.

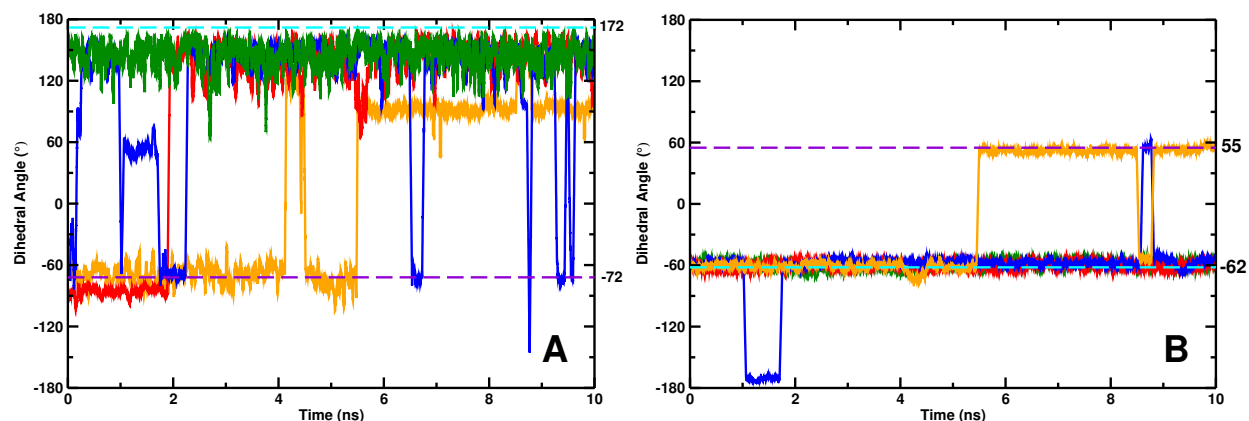


Figure S4: Panel A) Dihedral angle of $\angle C_{\alpha}C_{\beta}SN$ for Cys10 as a function of time in cis-MbSNO with PC (red), trans-MbSNO with PC (blue), cis-MbSNO with MTP (green) and trans-MbSNO with MTP (orange) at 300 K. Panel B) Dihedral angle $\angle NC_{\alpha}C_{\beta}S$ of Cys10 as a function of time in cis-MbSNO with PC (red), trans-MbSNO with PC (blue), cis-MbSNO with MTP (green) and trans-MbSNO with MTP (orange) at 300 K. Dashed lines represent the values from the major (cyan) and minor (violet) cis-MbSNO conformer in 2NRM.

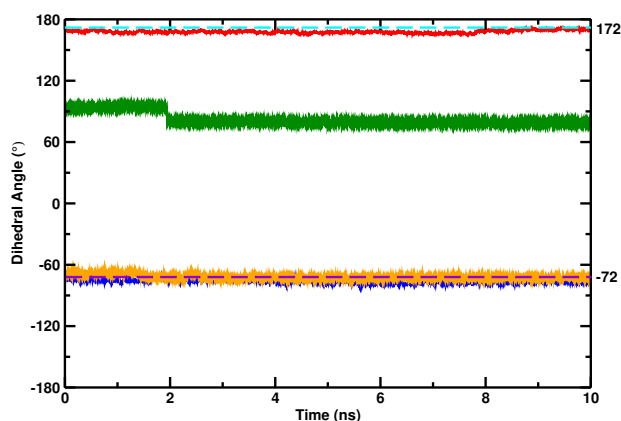


Figure S5: Dihedral angle of $\angle C_{\alpha}C_{\beta}SN$ for Cys10 as a function of time in cis-MbSNO with PC (red), trans-MbSNO with PC (blue), cis-MbSNO with MTP (green) and trans-MbSNO with MTP (orange) at 50 K. Dashed lines represent the values from the major (cyan) and minor (violet) cis-MbSNO conformer in 2NRM.

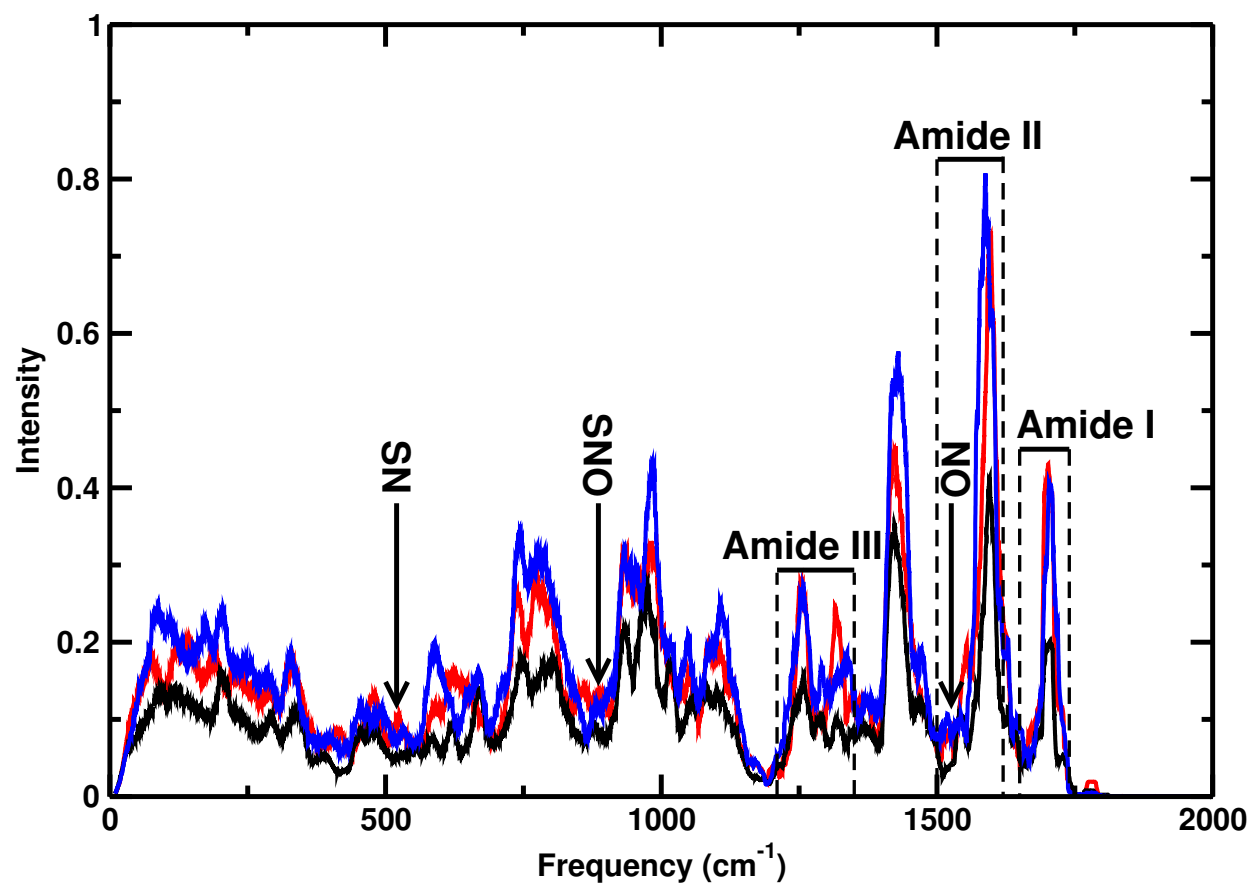


Figure S6: Infrared spectrum of WT (black), cis-MbSNO (red) and trans-MbSNO (blue) at 50 K from the total dipole moment of the protein.

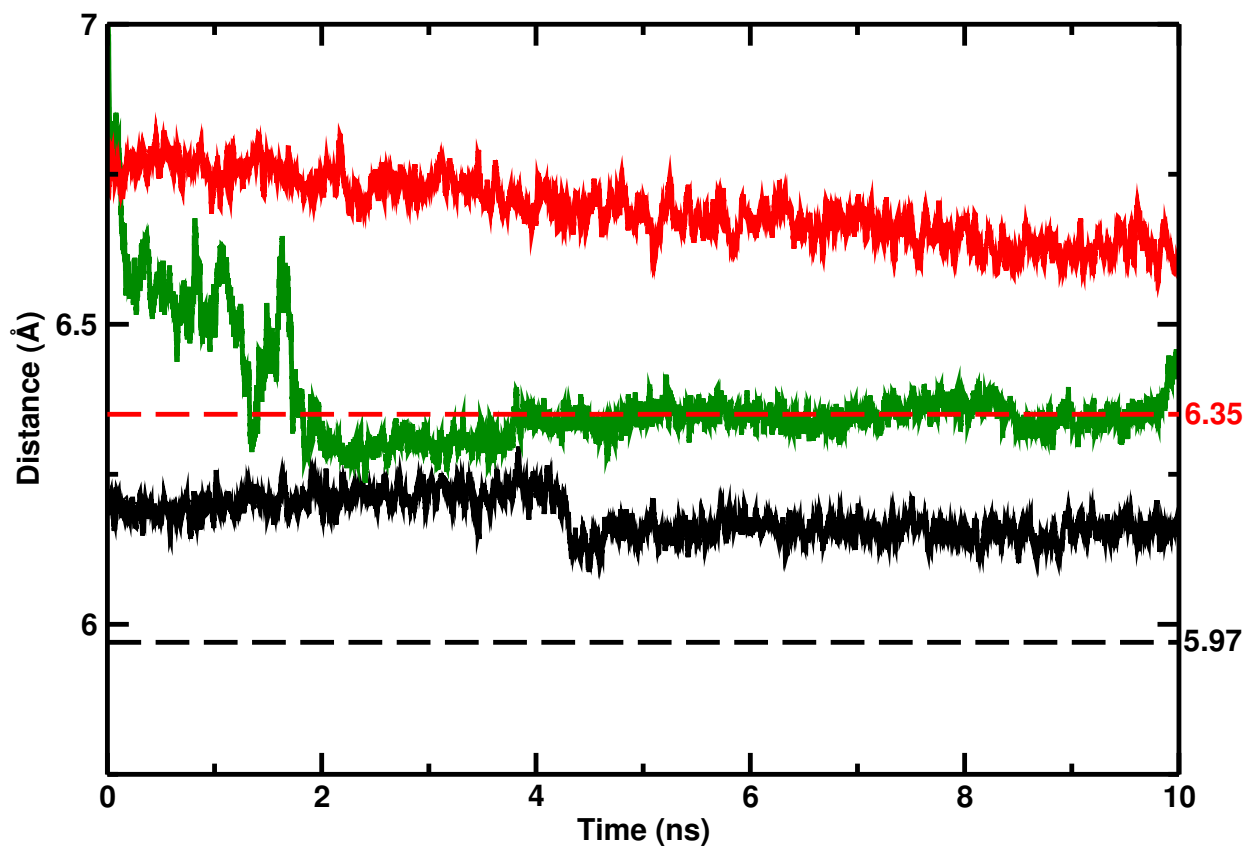


Figure S7: Distance between the C α of Cys10 and Ile117 residues in WT (black), cis-MbSNO with PC (red) and cis-MbSNO with MTP (green) at 50 K. Dash lines represents the Cys10 - Ile117 distance in the crystal structure of WT and major conformer of cis-MbSNO in 2NRM

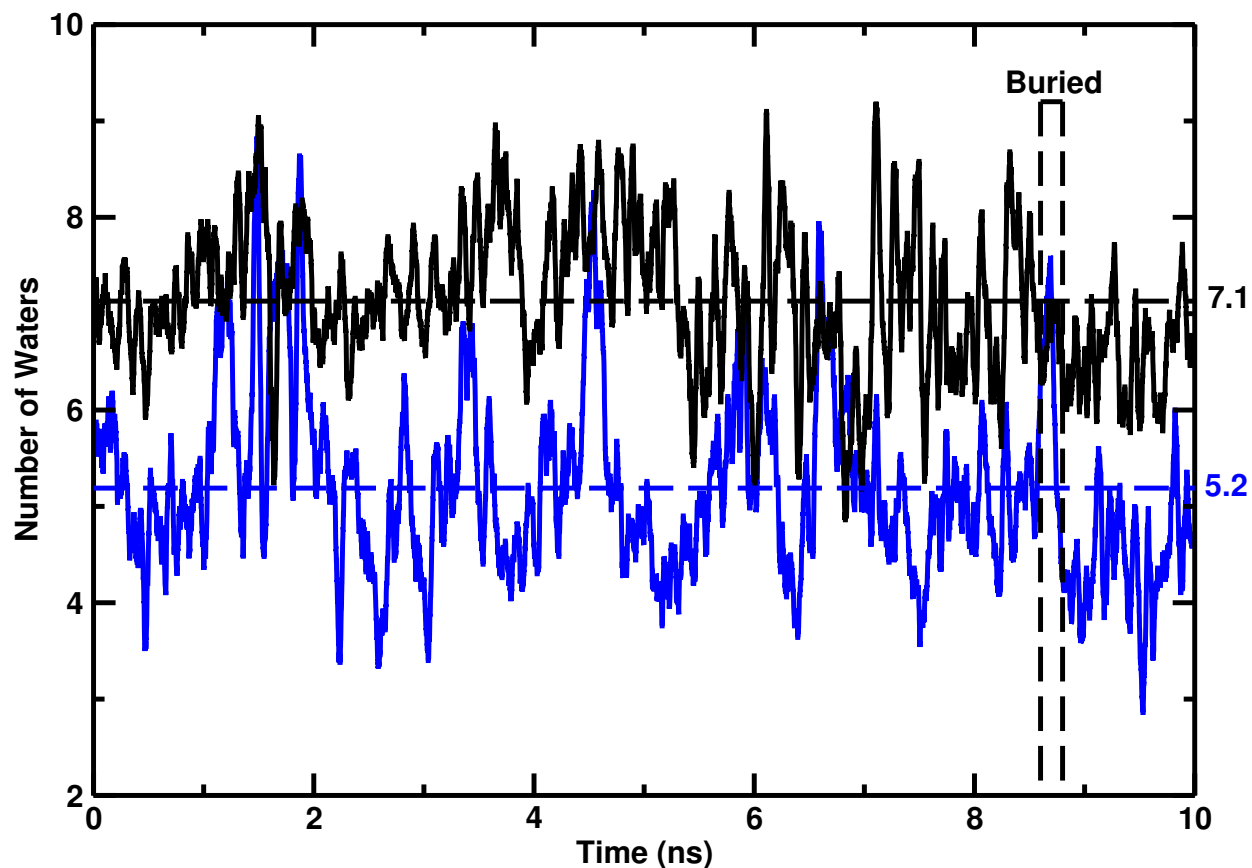


Figure S8: The number of water molecules between helices A and H and around loop GH. All water oxygen atoms within 5 Å of residues 5 to 12 (helix A) and residues 113 to 130 (loop GH, helix H) as a function of time are reported for WT (black) and trans-MbSNO (blue, simulation with PCs). The average occupation is 7.1 water molecules for WT compared with 5.2 for trans-MbSNO, i.e. a difference of 30 %.